https://doi.org/

Computational analysis of drinking behavior modeling through the Genocchi wavelet approach

Jasinth Sylvia[1] and Surath Ghosh[1]

[1]Department of Mathematics, SAS, Vellore Institute of Technology Chennai, Kellambakkam, Chennai, 600127, Tamilnadu, India
Corresponding author: surath.applied@gmail.com

Abstract. The modeling and analysis of drinking behavior in a population are addressed through a nonlinear mathematical system. Solutions are obtained by utilizing the Genocchi wavelet technique, and a detailed theoretical exploration of error bounds, convergence, existence, and uniqueness, as well as boundedness of the outcomes, is provided. The accuracy of the proposed Genocchi wavelet technique is demonstrated through an absolute error analysis by comparing its results, as well as those obtained via the Adams-Bashforth-Moulton method, with previously published solutions. Numerical simulations, including tabular results and graphical illustrations for different fractional orders, highlight the effectiveness of the proposed approach. Three-dimensional visualizations are employed to examine the influence of fractional-order variations on the system dynamics. Furthermore, alcohol consumption data from Brunei over the period 2000-2020 are analyzed to support the practical relevance of the model.

Key words: Drinking behavior model; Genocchi wavelet; Convergent analysis; Adams Bashforth Moulton method
Received: 4 January 2026 **Revised:** 22 January 2026 **Accepted:** 27 January 2026

1. Introduction

Fractional calculus (FC) can be seen as both an ancient as well as emerging field. It is considered ancient due to its origins in the thoughts of G.W. Leibniz in 1697 as well as L. Euler in 1730, with continuous development up to the present. However, its emergence as a novel subject has been recognized only since the 1970s, when FC began to be addressed through specialized conferences and treatises. The initial conference exclusively for FC was organized under the coordination of B. Ross in 1974 at the University of New Haven. Later, a growing number of books and journals on fractional calculus and its applications have been produced, a trend expected to continue in the future. FC enables derivatives as well as integrals of any non negative real order. The term 'fractional' is maintained due to historical context. The field of fractional calculus has gained significant attention over the past three decades, with substantial contributions made by scientists through the introduction of various fractional operators. The importance of FC continues to grow, as evidenced by its expanding range of applications and ongoing research advancements. More realistic results are provided by modern calculus compared to classical approaches. Numerous research articles, books, and monographs have been published and exploring this area. The dynamics of real-world phenomena have been

systematically investigated using arbitrary-order approaches for classical differentiation and integration models. It was found that fractional-order models accurately described both the passion fruit seed drying process and lipid extraction kinetics. Super diffusion ($\alpha > 1$) was observed during drying, while sub diffusion ($\alpha < 1$) was identified during lipid extraction, indicating deviation from Fick's law in [34]. A variable non integer order rheological framework has been introduced to explain the development of mechanical characteristics and stress-strain behavior in rock while the flow of plastic. This model is defined by five parameters, is used to capture the hardening and softening effects of rock under varying confining pressures and provides a smooth function of plastic strain is enabled in [20]. The fractional order kinetic model is presented for estimating the highest methane yield as well as degradation kinetics in bio-methane potential assays, demonstrating superior performance over first-order models in capturing methane production complexities and managing substrate heterogeneity. Its effectiveness is shown across various digestion scenarios, with computations simplified for fractional orders above 0.8 is mentioned in [11]. The Hepatitis model is reformulated from integer to non integer order in the sense of Caputo derivative as well as the Katugampola derivative is introduced and analyzed. Solutions are derived using homotopy perturbation transform method in [17]. The fractional-order HIV framework is represented by utilizing the Atangana-Baleanu (AB) operator, emphasizing its significance in biological science. Solutions are analyzed for varying fractional orders using the numerical techniques, including the Adams-Bashforth and Euler methods. The distinctiveness of the outcomes is demonstrated through the Banach fixed point theorem in [36]. A predator-prey system with two prey species is modeled using a two step non integer order Adams-Bashforth technique based on the AB operator in the sense of Caputo. The dynamics of the system are analyzed locally and the distinctiveness as well as the uniqueness of outcomes are established by utilizing the fixed point theorem. The convergence of the scheme is verified and the dynamic wave phenomena are demonstrated numerically for varying fractional induces, providing ecological insights in [28].

The drinking behavior model has been extensively studied to understand the dynamics of alcohol consumption patterns within a population. An important factor to consider when studying alcohol drinking is the inclination of certain people to gently raise their alcohol intake under stressful or depressive conditions, independent of social influences. The proposed model uses a simplified three compartment framework to examine the impact of public interactions on drinking behavior. It assumes that mobility between compartments depends on the populations of both the source and destination compartments, except for a competing spontaneous probability driving transitions from moderate to risk consumption. The model follows an epidemic-like structure, with transitions governed by probabilities under the assumption of homogeneous mixing a entirely connected people of $\mathcal{N}$ individuals. The individuals is categorized into three groups:

S : Non consumers who have either never consumed alcohol or have quit. These individuals are susceptible to becoming alcohol consumers, either for the initial stage or by relapsing.

M : Non risk consumers who engage in regular low-level alcohol consumption, referred to as moderate consumers.

R : Risk drinkers characterized by systematic high level alcohol drinkers, mentioned as risk drinkers.

In our framework, 'b' symbolizes the probability of a Moderate or risk drinker influencing a susceptible individual to become a drinker. Similarly, 's' denotes the probability of risk drinkers turning moderate drinkers into risk drinkers via social interaction. The transition of moderate drinker into risk drinker can also occur spontaneously, with probability 'a' representing self induced progression due to factors like stress or depression, independent of social interaction. The recovery probability 'v' reflects the impact of non drinkers in helping risk

alcohol consumers to quit drinking. Transitions from risk drinker into moderate drinker are considered negligible in this model, as excessive drinkers are assumed unlikely to revert to moderate drinking through interaction with moderate drinker individuals, while susceptible individuals exert greater influence to cease drinking [10].

$$\begin{aligned}
\frac{dS(\mathfrak{t})}{d\mathfrak{t}} &= -b(S(\mathfrak{t})M(\mathfrak{t})) - b(S(\mathfrak{t})R(\mathfrak{t})) + v(S(\mathfrak{t})R(\mathfrak{t})),\\
\frac{dM(\mathfrak{t})}{d\mathfrak{t}} &= b(S(\mathfrak{t})M(\mathfrak{t})) + b(S(\mathfrak{t})R(\mathfrak{t})) - s(M(\mathfrak{t})R(\mathfrak{t})) - a(M(\mathfrak{t})),\\
\frac{dR(\mathfrak{t})}{d\mathfrak{t}} &= a(M(\mathfrak{t})) + s(M(\mathfrak{t})R(\mathfrak{t})) - v(S(\mathfrak{t})R(\mathfrak{t})).
\end{aligned}$$

$$S(0) = 0.99 = \mathcal{I};\ M(0) = 0.01 = \mathcal{J};\ R(0) = 0 = \mathfrak{K};$$

Using the Caputo fractional derivative in the drinking behavior model enhances its ability to capture memory effects and cumulative influences, essential in modeling addiction and recovery. Fractional-order models provide smoother transitions and better reflect real-world dynamics compared to integer-order models. This approach enables a more accurate depiction of phase transitions and coexistence of sub populations. Additionally, it broadens the model's applicability to studies involving delayed interventions and complex social interactions. Overall, it enriches the model's predictive power and realism.

$$\begin{aligned}
{}^{c}D_0^{\alpha} S(\mathfrak{t}) &= -b(S(\mathfrak{t})M(\mathfrak{t})) - b(S(\mathfrak{t})R(\mathfrak{t})) + v(S(\mathfrak{t})R(\mathfrak{t}))\\
{}^{c}D_0^{\alpha} M(\mathfrak{t}) &= b(S(\mathfrak{t})M(\mathfrak{t})) + b(S(\mathfrak{t})R(\mathfrak{t})) - s(M(\mathfrak{t})R(\mathfrak{t})) - a(M(\mathfrak{t}))\\
{}^{c}D_0^{\alpha} R(\mathfrak{t}) &= a(M(\mathfrak{t})) + s(M(\mathfrak{t})R(\mathfrak{t})) - v(S(\mathfrak{t})R(\mathfrak{t})).
\end{aligned}$$

During the 1980s, wavelet analysis emerged as a powerful tool with remarkable implementations in picture processing, processing of signals and various fields of research. Wavelets are defined as unique oscillatory behavior functions with compact help as well as the capability to convey the functions at different phases of resolution. In recent years, numerous wavelet techniques have been developed for enabling the solution of a vast areas of fractional differential equations (FDEs) as well as fractional integro differential equations (FIDEs). Their versatility has been demonstrated through widespread applications across diverse scientific and engineering disciplines. In particular, wavelet bases have been widely utilized for numerically solving complex problems. The [18] presents an efficient Haar wavelet method to solve Fisher's equation, a key reaction diffusion equation with results characterized by steep propagating fronts at high reaction rates. The global impact of communicable disease like Herpes, Rubella, Chagas, Hepatitis B and AIDS is addressed, with their transmission and economic burden noted. A non integer order SEIR framework with a variable population is used and a Haar wavelet-based numerical method is proposed for efficiency and accuracy [31]. The spread of computer viruses in vulnerable networks and their mitigation using kill signal nodes are analyzed through a non integer order SIRA framework with Caputo operator. The existence as well as the uniqueness of the results are established by utilizing fixed point theories of Schauder and Banach. A numerical algorithm, based on Broyden's technique as well as the Haar collocations technique are developed in [41]. The chaotic behavior of atmospheric systems is explored using the Bernoulli wavelet collocation technique, applied to a model that analyzing greenhouse gases, temperature, and permafrost thaw. The Bernoulli wavelet (BW) technique's superiority as well as efficiency are highlighted through numerical results, compared to techniques including forward Euler, Adam-Bashforth as well as fde12 solvers in [2].

The BW method is applied to three biological models: COVID-19, dengue fever, and tuberculosis. These three models, represented as systems of coupled differential equations. The derived results are compared with other numerical techniques like Runge-Kutta as well as the ND solvers. Improved accuracy as well as the convergence are demonstrated by the BW technique is in [25]. BW are used to solve fractional-order financial chaotic systems by converting differential equations into algebraic ones. The system models the price indexes, interest rates, and investment demand, accounting for memory and chaos. Stability, convergence, and residual errors are also analyzed, proving the BW method's accuracy and effectiveness for financial problem-solving in [5]. The properties of shifted Legendre polynomials are explored in the paper and the new operational matrices based on them are developed. These matrices are utilized to approximate the outcomes of coupled FDE systems with boundary conditions and the problems are resolved to illustrate the accuracy of the shifted Legendre wavelet technique. The technique is computer-based and it is implemented in MATLAB are presented in [21]. An iterative spectral method for solving Lane-Emden (LE) equations is presented, using an extended Legendre wavelet. The Gauss-Legendre collection points are collected. Using this strategy, the differential non linear equations is transforms into a set of algebraic non linear equations. By resolving the obtained algebraic non linear equations, an approximate outcomes for the LE equation is executed in [14]. A numerical technique built upon Chebyshev wavelets is developed for solving FDEs. The operational matrix for fractional derivatives is also derived, simplifying the problem into algebraic equations, as demonstrated by illustrative examples in [6]. Numerical algorithms are developed using tau and collocation methods to solve higher order singular equations, particularly of the Emden Fowler type, through the use of refined Chebyshev polynomials of the third type. Convergence is analyzed, and examples are provided to demonstrate the accuracy as well as efficiency discussed in [1].

The wavelet method shows rapid convergence with a high convergence rate, while ABM method needs more iterations to achieve convergence, and it allows simultaneous time-frequency analysis. Genocchi wavelets are derived using Genocchi polynomials and are employed for solving differential equations and signal processing problems. The Genocchi wavelets exhibit numerous advantageous properties over a defined interval. Notably, the coefficients of the factors in Genocchi polynomials are distinctively whole numbers, ensuring the elimination of computational errors. In contrast, the coefficients of factors in many other polynomials like the Legendre polynomials as well as the Bernoulli polynomials do not represent integer values. This characteristic highlights the superiority of Genocchi polynomials over Bernoulli polynomials. Furthermore, it is observed that the factors in Genocchi polynomials are fewer compared to those in other polynomials. For instance, the Genocchi polynomial $G_6(t)$ consists of four factors, while the Bernoulli polynomial $B_6(t)$ contains five factors. Similarly, the shifted Chebyshev polynomial $T_6(t)$ as well as the shifted Legendre polynomial $L_6(t)$ each include seven terms. Consequently, less CPU time is required when approximating a function using Genocchi polynomials compared to Bernoulli, shifted Chebyshev, or shifted Legendre polynomials in [33].

The Adams-Bashforth-Moulton (ABM) technique is recognized as a predictor-corrector technique applied numerically to solve ordinary differential equations (ODEs). The explicit Adams-Bashforth technique (AB) is combined with the implicit Adams-Moulton technique (AM). This approach is designed to enhance accuracy and stability of the systems. A new numerical technique built up on Genocchi wavelets has been introduced for resolving the arbitary order SEIR measles framework using the Caputo derivative. The problem is simplified into algebraic non linear equations through the combination of an operational matrix and the collocation method. The solutions are compared with the ABM scheme to evaluate accuracy. Graphical results, along with error and convergence analyses, are provided to validate the

method's effectiveness in modeling disease dynamics in [24]. The [30] focuses on the solution of differential Riccati equations using AB and AM methods. Solutions are explicitly computed using AB, while algebraic Riccati equations are solved in AM through Newton's technique. Nine different algorithms are being evaluated to solve the problem, including Sylvester, GMRES, fixed-point, and combined methods, allowing a flexible and efficient approach to be applied depending on the problem's requirements. The multiplicative version of ABM algorithms is proposed for the approximate outcomes of multiplicative differential equations. The truncation error approximation is discussed for these numerical algorithms. The stability characteristics of these techniques are also examined by utilizing the standard test equation in [27]. A new spectral-time fractional ABM method is proposed for solving fractional partial differential equations, with spectral techniques. The stability as well as the spectral accuracy of the method are demonstrated through analysis and examples in [38]. Wireless sensor networks are widely used for tasks such as monitoring and surveillance, with efficiency enhanced by information prediction schemes. The ABM algorithm is proposed to improve prediction accuracy when compared to the Milne Simpson scheme in [19]. Methods for solving FDEs and approximating Caputo fractional derivatives are introduced using reproducing kernel Hilbert spaces (RKHSs), including a Mittag-Leffler. A modified ABM method is also proposed for these tasks [35]. The Lotka-Volterra model is solved using the spectral method with shifted Chebyshev polynomials and the ABM method. A comparison between the two approaches is conducted, highlighting efficiency of the results in two case studies are represented in [16]. A new three-step trigonometrically fitted ABM predictor-corrector method is introduced, utilizing a third-order predictor and a third-order corrector. Its efficiency in solving first-order periodic initial value problems is demonstrated through numerical experiments in [32]. The precise numerical integration of the Moon's motion, modeled as a delay differential equation (DDE) due to tidal forces is addressed. Forward integration of DDEs is well-established, while backward integration transforms the problem into an advanced differential equation. A modified ABM method is explored for integrating the Moon's DDE in both time directions is showcased in [3]. The SIR model for simulating COVID-19 in Malaysia is analyzed using the Caputo derivative applied and solved through the ABM method. The results are validated using the Runge-Kutta method, and fractional derivative orders above 0.5 are shown to be reliable in [4].

The dynamics of drinking behavior within a population are considered as vital for the development of effective public health interventions and policies. These dynamics are influenced by psychological stressors and recovery mechanisms are required to be modeled and analyzed using advanced mathematical tools for greater accuracy. By employing fractional derivatives in the sense of Caputo is a more realistic and nuanced representation of addiction and recovery dynamics in a long term behavioral trends. The Genocchi wavelet method is utilized in this work is an innovative approach for solving the fractional order drinking behavior model. The outcomes of this research are offering future researchers a robust methodology for extending fractional order modeling to other behavioral, ecological systems, epidemiology, environmental modeling and social economic analyses. Additionally, the reliability of the Genocchi wavelet approach are validated through a comparative analysis with the Adams Bashforth Moulton method setting a benchmark for future studies.

The novelty of the work is the previously published integer-order system has been reformulated into a fractional-order model to account for memory effects and achieve improved computational accuracy. The resulting system has been solved using an advanced numerical approach based on the GW method. Enhanced accuracy has been observed in the results, and the superior performance of the GW method has been confirmed through comparison with existing numerical techniques.

The paper begins with an introduction, where the basics of fractional calculus, the drinking behavior model, the Genocchi wavelet method, and the ABM technique are discussed, along with the motivation for the study. In Section 2, the Preliminaries of FC are provided, including definitions of fractional integral and derivative in the Riemann-Liouville and Caputo senses. In Section 3, the Genocchi Wavelet is introduced, with its properties and constructed using Genocchi polynomials. The Genocchi wavelet operational matrix is developed in Section 4, using block pulse functions is described. In Section 5, an Error and convergence analysis is presented, including error bounds and proof of uniform convergence. In the Sections 6 and 7, the existence and uniqueness and boundedness of solutions are established. The application of the Genocchi wavelet method to solve the drinking behavior model is carried out in Section 8, and in Section 9, the ABM technique is applied for comparative analysis. A Numerical Discussion is presented in Section 10, with graphical results, comparisons across fractional orders, error analysis, and 3D visualizations of the model's dynamics included. Finally, in the section 11, the findings are summarized with conclusion statement.

2. Preliminaries of fractional calculus (FC)

In this part, the basic definitions of FC is discussed as follows [7, 9, 15, 23, 37, 39];

Definition 1. *The Riemann-Liouville non-integer order integral of a function $S(t)$ of order $\alpha \geq 0$ can be declared as follows,*

$$I_0^{\alpha} S(\mathfrak{t}) = \frac{1}{\Gamma(\alpha)} \int_0^{\mathfrak{t}} (\mathfrak{t} - \beta)^{\alpha - 1} S(\beta)\, d\beta,$$

Definition 2. *The non integer order derivative of a function $S(t)$ of order α in the Caputo operator is stated as follows,*

$$^{c}D_0^{\alpha} S(\mathfrak{t}) = I_0^{m-\alpha}(\frac{d^m S}{dt^m})(\mathfrak{t}),$$

$$^{c}D_0^{\alpha} S(\mathfrak{t}) = \frac{1}{\Gamma(m-\alpha)} \int_0^{\mathfrak{t}} (\mathfrak{t} - \beta)^{m-\alpha-1} \frac{d^m S}{d\beta^m}(\beta) d\beta,$$

The following are the basic properties

$$^{c}D_0^{\alpha}(I_0^{\alpha} S)(\mathfrak{t}) = S(\mathfrak{t}),$$

$$I_0^{\alpha}(^{c}D_{\mathfrak{t}}^{\alpha} S)(\mathfrak{t}) = S(\mathfrak{t}) - \sum_{k=0}^{m-1} \frac{d^k S}{d\mathfrak{t}^{\mathfrak{t}}}(0^{+}) \frac{\mathfrak{t}^k}{k!}.$$

3. Definition of Genocchi wavelet

The Genocchi wavelets $\Upsilon_{nm}(\mathfrak{t})$ are characterized over the region $[0, \mathfrak{t}_l)$ in the following manner:

$$\Upsilon_{nm}(\mathfrak{t}) = \begin{cases} \frac{2^{\mathcal{K}-1}}{\sqrt{\mathcal{R}(m)}} \mathcal{GP}_m \left(2^{\mathcal{K}-1}\mathfrak{t} - n + 1\right), & \text{if } \frac{n-1}{2^{\mathcal{K}-1}}\mathfrak{t}_l \leq \mathfrak{t} < \frac{n}{2^{\mathcal{K}-1}}\mathfrak{t}_l, \\ 0, & \text{otherwise,} \end{cases}$$

here k and M are non negative integers and $\mathcal{R}(m)$ is described as

$$\mathcal{R}(m) = \frac{2(-1)^m (m!)^2}{(2m)!} \mathcal{GN}_{2m},$$

here $m = 1, 2, \ldots, M$, $n = 1, 2, \ldots, 2^{\mathcal{K}-1}$, and $\mathcal{GN}_{2m}$ is the Genocchi number. The $\mathcal{GP}(\mathfrak{t})$ represents the Genocchi polynomials, that contain values:

$$\begin{aligned}
\mathcal{GP}_0(\mathfrak{t}) &= 0,\\
\mathcal{GP}_1(\mathfrak{t}) &= 1,\\
\mathcal{GP}_2(\mathfrak{t}) &= 2\mathfrak{t} - 1,\\
\mathcal{GP}_3(\mathfrak{t}) &= 3\mathfrak{t}^2 - 3\mathfrak{t},\\
\mathcal{GP}_4(\mathfrak{t}) &= 4\mathfrak{t}^3 - 6\mathfrak{t}^2 + 1.
\end{aligned}$$

The first few Genocchi numbers are

$$\mathcal{GN}_0 = 0, \quad \mathcal{GN}_1 = 1, \quad \mathcal{GN}_2 = -1, \quad \mathcal{GN}_3 = 0, \quad \mathcal{GN}_4 = 1, \quad \mathcal{GN}_5 = 0, \quad \mathcal{GN}_6 = -3.$$

Let $\Omega_{k,M}$ denote the space spanned by the Genocchi wavelets Υ_{nm},

$$\Omega_{k,M} = \text{span}\{\Upsilon_{1,1}, \Upsilon_{2,1}, \ldots, \Upsilon_{2^{k-1},1}, \Upsilon_{1,2}, \ldots, \Upsilon_{2^{k-1},2}, \ldots, \Upsilon_{2^{k-1},M}\} \subset L^2(0, \mathfrak{t}_l).$$

Furthermore, let us consider $\mathcal{U}$ be an random element in the $L^2(0, \mathfrak{t}_l)$, after that Υ has an distinct best approximation out of $\Omega_{k,M}$, $\ni \mathcal{U}_0 \in \delta_{k,M}$, satisfying

$$\forall \zeta \in \delta_{k,M}, \|\mathcal{U} - \mathcal{U}_0\| \leq \|\mathcal{U} - \zeta\|.$$

Since $\mathcal{U}_0 \in \delta_{k,M}$ is the distinct element of Υ, $\exists$ distinct coefficients such that

$$\mathcal{U}(\mathfrak{t}) \approx \mathcal{U}_0(\mathfrak{t}) = \sum_{n=1}^{2^{k-1}} \sum_{m=1}^{M} \lambda_{n,m} \Upsilon_{nm}(\mathfrak{t}) = \Lambda^T \Upsilon(\mathfrak{t}),$$

where

$$\Lambda^T = [\lambda_{1,1}, \ldots, \lambda_{2^{k-1},1}, \lambda_{1,2}, \ldots, \lambda_{2^{k-1},2}, \ldots, \lambda_{2^{k-1},M}].$$

Additionally,

$$\Upsilon(\mathfrak{t}) = \{\upsilon_{1,1}, \upsilon_{2,1}, \ldots, \upsilon_{2^{k-1},1}, \upsilon_{1,2}, \ldots, \upsilon_{2^{k-1},2}, \ldots, \upsilon_{2^{k-1},M}\}.$$

The collocation points are chosen as

$$\mathfrak{t}_i = \frac{2i-1}{2\hat{m}} \mathfrak{t}_l, \quad i = 1, 2, \ldots, \hat{m} = 2^{\mathcal{K}-1} M,$$

we obtain the required matrix as

$$\Upsilon_{\hat{m} \times \hat{m}} = \begin{pmatrix}
1.4142 & 1.4142 & 1.4142 & 0 & 0 & 0\\
0 & 0 & 0 & 1.4142 & 1.4142 & 1.4142\\
-1.6330 & 0 & 1.6330 & 0 & 0 & 0\\
0 & 0 & 0 & -1.6330 & 0 & 1.6330\\
-1.0758 & -1.9365 & -1.0758 & 0 & 0 & 0\\
0 & 0 & 0 & -1.0758 & -1.9365 & -1.0758
\end{pmatrix}.$$

Here $\mathcal{K} = 2$, $M = 3$.

4. Genocchi wavelet operational matrix

In this section, the Genocchi wavelet operational matrix (GWOM) is obtained by using a block pulse.

4.1. The Block Pulse

The block pulse are characterized over the region $[0, t_l)$ as follows [22, 40]

$$\mathcal{B}(\mathfrak{t}) = \begin{cases} 1, & \text{if } \frac{j\mathfrak{t}_l}{\hat{m}} \leq \mathfrak{t} < \frac{(j+1)\mathfrak{t}_l}{\hat{m}}, \\ 0, & \text{otherwise,} \end{cases} \tag{1}$$

where $j = 0, 1, 2, \ldots, \hat{m}$.

$$(I^{\alpha}_{\mathfrak{t}}\mathcal{B}_{\hat{m}})(\mathfrak{t}) \approx F^{\alpha}\mathcal{B}_{\hat{m}}, \tag{2}$$

where

$$F^{\alpha}_{\hat{m}\times\hat{m}} = \frac{\mathfrak{t}^{\alpha}_l}{\hat{m}^{\alpha}\Gamma(\alpha+2)} \begin{pmatrix} 1 & \mathcal{P}_1 & \mathcal{P}_2 & \cdots & \mathcal{P}_{\hat{m}-1} \\ 0 & 1 & \mathcal{P}_1 & \cdots & \mathcal{P}_{\hat{m}-2} \\ 0 & 0 & 1 & \cdots & \mathcal{P}_{\hat{m}-3} \\ \vdots & \vdots & \vdots & \ddots & \vdots \\ 0 & 0 & 0 & \cdots & 1 \end{pmatrix},$$

and $\mathcal{P}_{\mathcal{L}} = (\mathcal{L}+1)^{\alpha+1} - 2\mathcal{L}^{\alpha+1} + (\mathcal{L}_1 - 1)^{\alpha+1}$ for $\mathcal{L} = 1, 2, 3, \ldots, \hat{m} - 1$.

Now, we develop the GWOM for non integer order integration $\mathcal{P}^{\alpha}$. Let

$$(I^{\alpha}_{\mathfrak{t}}\Upsilon)(\mathfrak{t}) \approx \mathcal{P}^{\alpha}\Upsilon(\mathfrak{t}). \tag{3}$$

Thus, we have

$$\mathcal{P}^{\alpha} = \Upsilon_{\hat{m}\times\hat{m}} F^{\alpha} \Upsilon^{-1}_{\hat{m}\times\hat{m}}. \tag{4}$$

Utilizing the aforesaid facts, the GWOM $\mathcal{P}^{\alpha}$ is defined for $\alpha = 0.7$, $M = 3$, $\mathcal{K} = 2$, and $\mathfrak{t}_l = 30$ as follows

$$\mathcal{P}^{\alpha}_{6\times 6} = \begin{bmatrix} 6.0164 & 11.0289 & 3.3603 & -0.3890 & -0.2541 & 0.1906 \\ 0 & 6.0164 & 0 & 3.3603 & 0 & -0.2541 \\ 0.9839 & 0.4652 & 0.4666 & -0.1410 & 4.1211 & 0.1239 \\ 0 & 0.9839 & 0 & 0.4666 & 0 & 4.1211 \\ -5.5673 & -10.5985 & -3.6196 & 0.3634 & 0.5053 & -0.1700 \\ 0 & -5.5673 & 0 & -3.6196 & 0 & 0.5053 \end{bmatrix}.$$

5. Error and Convergence analysis

5.1. Error analysis

Theorem 1. *Consider* $\mathcal{U}(\mathfrak{t}) \in C^M[0,1]$, $\Lambda^T\Upsilon(\mathfrak{t})$ *be the numerical outcomes by utilizing Genocchi wavelets. Then the error bound is given as:*

$$\|\mathcal{E}(\mathfrak{t})\| \leq \frac{2}{M!2^{M(\mathcal{K}+1)}} \max_{\mathfrak{t}\in[0,1]} |\mathcal{U}^{(M)}(\mathfrak{t})|. \tag{5}$$

Proof. Utilizing the characteristic of the norm, we get:

$$\|\mathcal{E}(\mathfrak{t})\|^2 = \int_0^1 |\mathcal{U}(\mathfrak{t}) - \Lambda^T \Upsilon(\mathfrak{t})|^2 d\mathfrak{t}.$$

Divide the range $[0,1]$ into 2^{k-1} sub ranges:

$$I_n = \left[\frac{n-1}{2^{\mathcal{K}-1}}, \frac{n}{2^{\mathcal{K}-1}}\right], \quad n = 1, 2, \ldots, 2^{\mathcal{K}-1}.$$

Thus,

$$\|\mathcal{E}(\mathfrak{t})\|^2 = \sum_{n=1}^{2^{\mathcal{K}-1}} \int_{I_n} |\mathcal{U}(\mathfrak{t}) - \Lambda^T \Upsilon(\mathfrak{t})|^2 d\mathfrak{t}.,$$

$$\|\mathcal{E}(\mathfrak{t})\|^2 = \sum_{n=1}^{2^{\mathcal{K}-1}} \int_{I_n} |\mathcal{U}(\mathfrak{t}) - \mathcal{P}_M(\mathfrak{t})|^2 d\mathfrak{t},$$

where $\mathcal{P}_M(\mathfrak{t})$ is the polynomial with degree M that interpolates $\mathcal{U}(\mathfrak{t})$ on each I_n.

By utilizing the maximum error approximates for polynomials, we have:

$$\|\mathcal{E}(\mathfrak{t})\|^2 \leq \sum_{n=1}^{2^{\mathcal{K}-1}} \int_{I_n} \frac{2}{M! 2^{M(\mathcal{K}+1)}} \max_{\mathfrak{t} \in I_n} |\mathcal{U}^{(M)}(\mathfrak{t})|^2 d\mathfrak{t}.$$

$$\|\mathcal{E}(t)\|^2 = \int_0^1 \left\| \frac{2}{M! 2^{M(k+1)}} \max_{\ell \in [0,1]} \|\mathcal{U}^{(M)}(\mathfrak{t})\| \right\|^2 dt,$$

we obtain:

$$\|\mathcal{E}(\mathfrak{t})\| \leq \frac{2}{M! 2^{M(\mathcal{K}+1)}} \max_{\mathfrak{t} \in [0,1]} |\mathcal{U}^{(M)}(\mathfrak{t})|.$$

Hence the results is proved. □

5.2. Convergence analysis

Theorem 2. *If $\mathcal{U}(\mathfrak{t})$ is a smooth as well as bounded function $\in L^2[0,1)$, then the elaboration of $\mathcal{U}(\mathfrak{t})$ by utilizing Genocchi wavelets is converges uniformly.*

Proof. Assume $\mathcal{U}(\mathfrak{t})$ is a real valued bounded function specified on the region $[0,1)$. The coefficients associated with the Genocchi wavelets are expressed as follows:

$$\lambda_{nm} = \int_0^1 \mathcal{U}(\mathfrak{t}) \Upsilon_{nm} d\mathfrak{t} = \int_{\frac{n-1}{2^{k-1}}}^{\frac{n}{2^{\mathcal{K}-1}}} \mathcal{U}(\mathfrak{t}) 2^{\frac{k-1}{2}} \frac{1}{\sqrt{\mathcal{R}(m)}} \mathcal{GP}_m \left(2^{\mathcal{K}-1}\mathfrak{t} - n + 1\right) d\mathfrak{t}.$$

$$= \int_0^1 \mathcal{U}\left(\frac{y+n-1}{2^{\mathcal{K}-1}}\right) 2^{\frac{\mathcal{K}-1}{2}} \frac{1}{\sqrt{\mathcal{R}(m)}} \mathcal{GP}_m(y) 2^{1-k}\, dy.$$

Replacing $y = 2^{\mathcal{K}-1}t - n + 1$, we get

$$\lambda_{nm} = \frac{1}{2^{\mathcal{K}-1}} \frac{1}{\sqrt{\mathcal{R}(m)}} \int_0^1 \mathcal{U}\left(\frac{y+n-1}{2^{\mathcal{K}-1}}\right) \mathcal{GP}_m(y) dy.$$

By utilizing the mean value theorem for integrals, $\exists\ \xi \in [0,1) \ni$

$$\lambda_{nm} = \frac{1}{2^{\mathcal{K}-1}} \frac{1}{\sqrt{\mathcal{R}(m)}} \mathcal{U}\left(\frac{\xi+n-1}{2^{\mathcal{K}-1}}\right) \int_0^1 \mathcal{GP}_m(y)dy.$$

Let $\int_0^1 \mathcal{GP}_m(y)dy = B$ and $\mathcal{R}(m) > 0$, then

$$|\lambda_{nm}| \leq \frac{1}{2^{\mathcal{K}-1}} \frac{B}{\sqrt{\mathcal{R}(m)}} \left|\mathcal{U}\left(\frac{\xi+n-1}{2^{\mathcal{K}-1}}\right)\right|.$$

Given that $\mathcal{U}(\mathfrak{t})$ is a bounded function, it can be concluded that the series $\sum \lambda_{nm}$ is absolutely convergent.
$\implies \mathcal{U}(\mathfrak{t})$ is uniformly convergent. Hence, the required result is achieved. □

6. Existence and uniqueness

Theorem 3. *The non integer order drinking behavior model ensures the existence of a unique solution for all initial conditions that are non negative.*

Proof. To establish the sufficient criteria for the existence and uniqueness of results of a non integer order drinking behavior model in the region $\delta \times (0,T]$, here

$$\delta = \{(S,M,R) \in \mathcal{R}^3 : max(|S|,|M|,|R|) \leq \epsilon\}.$$

This approach is based on the methodology presented in [29]. At this stage, a map has been obtained.

$$\mathcal{A} = (\mathcal{A}_1(x), \mathcal{A}_2(x), \mathcal{A}_3(x)),$$

$$\mathcal{A}_1(x) = -b(S(\mathfrak{t})M(\mathfrak{t})) - b(S(\mathfrak{t})R(\mathfrak{t})) + v(S(\mathfrak{t})R(\mathfrak{t})),$$

$$\mathcal{A}_2(x) = b(S(\mathfrak{t})M(\mathfrak{t})) + b(S(\mathfrak{t})R(\mathfrak{t})) - s(M(\mathfrak{t})R(\mathfrak{t})) - aM(\mathfrak{t}),$$

$$\mathcal{A}_3(x) = aM(\mathfrak{t}) + s(M(\mathfrak{t})R(\mathfrak{t})) - v(S(\mathfrak{t})R(\mathfrak{t})).$$

$\forall x, \bar{x} \in \delta$, with the help of above equation can be written as

$$\begin{aligned}
\|\mathcal{A}(x) - \mathcal{A}(\overline{x})\| &= |\mathcal{A}_1(x) - \mathcal{A}_1(\overline{x})| + |\mathcal{A}_2(x) - \mathcal{A}_2(\overline{x})| + |\mathcal{A}_3(x) - \mathcal{A}_3(\overline{x})|, \\
&= |-b\big(S(\mathfrak{t})M(\mathfrak{t})\big) - b\big(S(\mathfrak{t}) \times R(\mathfrak{t})\big) + v\big(S(\mathfrak{t})R(\mathfrak{t})\big) \\
&\quad - \big(-\bar{b}\big(\bar{S}(\mathfrak{t})\bar{M}(\mathfrak{t})\big) - b\big(\bar{S}(\mathfrak{t})\bar{R}(\mathfrak{t})\big) + v\big(\bar{S}(\mathfrak{t})\bar{R}(\mathfrak{t})\big)\big)| \\
&\quad + |b\big(S(\mathfrak{t})M(\mathfrak{t})\big) + b\big(S(\mathfrak{t})R(\mathfrak{t})\big) - s\big(M(\mathfrak{t})R(\mathfrak{t})\big) - aM(\mathfrak{t}) \\
&\quad - b\big(\overline{S}(\mathfrak{t})\overline{M}(\mathfrak{t})\big) + b\big(\overline{S}(\mathfrak{t})\overline{R}(\mathfrak{t})\big) - s\big(\overline{M}(\mathfrak{t})\overline{R}(\mathfrak{t})\big) - a\overline{M}(\mathfrak{t})| \\
&\quad + |aM(\mathfrak{t}) + s\big(M(\mathfrak{t})R(\mathfrak{t})\big) - v\big(S(\mathfrak{t})R(\mathfrak{t})\big) - a\overline{M}(\mathfrak{t}) \\
&\quad + s\big(\overline{M}(\mathfrak{t})\overline{R}(\mathfrak{t})\big) - v\big(\overline{S}(\mathfrak{t})\overline{R}(\mathfrak{t})\big)|, \\
\|\mathcal{A}(x) - \mathcal{A}(\overline{x})\| &= |-b\big((S-\bar{S})(M-\bar{M})\big) - b\big((S-\bar{S})(R-\bar{R})\big) \\
&\quad + v\big((S-\bar{S})(R-\bar{R})\big)|, \\
&\quad + |b\big((S-\bar{S})(M-\bar{M})\big) + b\big((S-\bar{S})(R-\bar{R})\big) \\
&\quad - s\big((M-\bar{M})(R-\bar{R})\big) - a(M-\bar{M})|, \\
&\quad + |a\big(M-\bar{M}\big) + s\big((M-\bar{M})(R-\bar{R})\big) - v\big((S-\bar{S})(R-\bar{R})\big)|, \\
&\quad \leq \mathcal{A}\|x-\bar{x}\|.
\end{aligned}$$

Where

$$\mathcal{A} = max\{-2b + v, 2b - s - a, a + s - v\}.$$

Thus, the Lipschitz condition is fulfilled by $\mathcal{A}(x)$ ensuring the uniqueness of the numerical results for the non integer order drinking behavior model. □

7. Boundedness

Theorem 4. *In the system modeling drinking behavior with non integer order, every solution remains uniformly bounded in* $\mathcal{R}^3_+$.

Proof. To define the function efficiently

$$\begin{aligned}
\mathcal{X} &= S(\mathfrak{t}) + M(\mathfrak{t}) + R(\mathfrak{t}) \\
{}^{C}_{0}D^{\alpha}_{\mathfrak{t}}\mathcal{X}(\mathfrak{t}) &= {}^{C}_{0}D^{\alpha}_{\mathfrak{t}}S(\mathfrak{t}) + {}^{C}_{0}D^{\alpha}_{\mathfrak{t}}M(\mathfrak{t}) + {}^{C}_{0}D^{\alpha}_{\mathfrak{t}}R(\mathfrak{t}) \\
&= -b(S(\mathfrak{t})M(\mathfrak{t})) - b(S(\mathfrak{t})R(\mathfrak{t})) + v(S(\mathfrak{t}) \times R(\mathfrak{t})), \\
&+ b(S(\mathfrak{t})M(\mathfrak{t})) + b(S(\mathfrak{t})R(\mathfrak{t})) - s(M(\mathfrak{t})R(\mathfrak{t})) - aM(\mathfrak{t}), \\
&+ aM(\mathfrak{t}) + s(M(\mathfrak{t})R(\mathfrak{t})) - v(S(\mathfrak{t})R(\mathfrak{t})).
\end{aligned}$$

Let us consider a non negative integer α_0 such that

$$\begin{aligned}
{}^{C}_{0}D^{\alpha}_{\mathfrak{t}}\mathcal{X}(\mathfrak{t}) + \alpha_0\mathcal{X} &= -b(S(\mathfrak{t})M(\mathfrak{t})) - b(S(\mathfrak{t})R(\mathfrak{t})) + v(S(\mathfrak{t})R(\mathfrak{t})) \\
&+ b(S(\mathfrak{t})M(\mathfrak{t})) + b(S(\mathfrak{t})R(\mathfrak{t})) - s(M(\mathfrak{t})R(\mathfrak{t})) \\
&- aM(\mathfrak{t}) + aM(\mathfrak{t}) + s(M(\mathfrak{t})R(\mathfrak{t})) - v(S(\mathfrak{t})R(\mathfrak{t})) \\
&+ \alpha_0 S(\mathfrak{t}) + \alpha_0 M(\mathfrak{t}) + \alpha_0 R(\mathfrak{t}). \\
&= S(\mathfrak{t})\big(- bM(\mathfrak{t}) - bR(\mathfrak{t}) + vR(\mathfrak{t}) + bM(\mathfrak{t}) + bR(\mathfrak{t}) - vR(\mathfrak{t}) + \alpha_0\big) \\
&+ M(\mathfrak{t})\big(- bS(\mathfrak{t}) + bR(\mathfrak{t}) + bS(\mathfrak{t}) - sR(\mathfrak{t}) + sR(\mathfrak{t}) + \alpha_0\big) \\
&+ R(\mathfrak{t})\big(- bS(\mathfrak{t}) + VS(\mathfrak{t}) + bS(\mathfrak{t}) - sM(\mathfrak{t}) + sM(\mathfrak{t}) - vS(\mathfrak{t}) + \alpha_0\big). \\
&\leq S(\mathfrak{t})\big(- bM(\mathfrak{t}) - bR(\mathfrak{t}) + vR(\mathfrak{t}) + bM(\mathfrak{t}) + bR(\mathfrak{t}) - vR(\mathfrak{t}) + \alpha_0\big).
\end{aligned}$$

Suppose,

$$\mathcal{F}(x) = S(t)\alpha_0, \text{ then the max of } \mathcal{F}(x)\, at\, S = \frac{1}{2\alpha_0},$$

leads to

$${}^{C}_{0}D^{\alpha}_{\mathfrak{t}}\mathcal{X}(\mathfrak{t}) + \alpha\mathcal{X} \leq \frac{1}{4\alpha_0^2}.$$

Assume the initial condition $\mathcal{X}(0) = \mathcal{X}_0$, then the above equation can be resolved as follows [26]

$$\begin{aligned}
\mathcal{X}(\mathfrak{t}) &\leq \mathcal{X}_0 E_{\alpha,\alpha}(-\alpha_0\mathfrak{t}^{\alpha}) + \frac{1}{4\alpha_0^2}\int_0^{\mathfrak{t}} (\mathfrak{t}-s)^{\alpha-1}E_{\alpha,\alpha} - \alpha_0(\mathfrak{t}-s)^{\alpha}ds, \\
&= \mathcal{X}_0 E_{\alpha,\alpha}(-\alpha_0\mathfrak{t}^{\alpha}) + \frac{1}{4\alpha_0^2}\int_0^{\mathfrak{t}} (\mathfrak{t}-s)^{\alpha-1}\sum_{k=0}^{\infty}\frac{-\alpha_0^k(\mathfrak{t}-s)^{\alpha}k}{\Gamma(k\alpha+\alpha)}ds, \\
&= \mathcal{X}_0 E_{\alpha,\alpha}(-\alpha_0\mathfrak{t}^{\alpha}) + \frac{1}{4\alpha_0^2}\sum_{k=0}^{\infty}\frac{-\alpha_0^k}{\Gamma(k\alpha+\alpha)}\int_0^{\mathfrak{t}} (\mathfrak{t}-s)^{\alpha k+\alpha-1}ds, \\
&= \mathcal{X}_0 E_{\alpha,\alpha}(-\alpha_0\mathfrak{t}^{\alpha}) + \frac{1}{4\alpha_0^2}\mathfrak{t}^{\alpha}E_{\alpha,\alpha+1}(-\alpha_0\mathfrak{t}^{\alpha}).
\end{aligned}$$

After that we calculate $E_{\alpha,\alpha}(-\alpha_0\mathfrak{t}^{\alpha})$ as follows [8]

$$E_{\alpha,\alpha}(-\alpha_0\mathfrak{t}^\alpha) = -\frac{1}{\Gamma(-\alpha)}\frac{1}{\Gamma(-\alpha_0^2)\mathfrak{t}^2\alpha} + o(\frac{1}{-\alpha_0^3\mathfrak{t}^3\alpha}),$$
$$\to 0 \text{ as } \mathfrak{t} \to \infty,$$

furthermore, we calculate the value of $\mathfrak{t}^\alpha E_{\alpha,\alpha+1}(-\alpha_0\mathfrak{t}^\alpha)$ as follows:

$$\mathfrak{t}^\alpha E_{\alpha,\alpha+1}(-\alpha_0\mathfrak{t}^\alpha) = \frac{1}{\alpha_0} - \frac{1}{\Gamma(1-\alpha(-\alpha_0^2)\mathfrak{t}^\alpha)} + o(\frac{1}{(-\alpha_0^3)\mathfrak{t}^3\alpha}),$$

$$\frac{1}{\alpha_0} \; as \; \mathfrak{t} \to \infty,$$

now, the resulting equation becomes,

$$\mathcal{X}(\mathfrak{t}) \leq \frac{1}{4\alpha_0^3}.$$

As a result, all outcomes of the arbitrary order model in R_+^3 are confined to this region,

$$\chi = \{(S, M, R) \in R_+^3 : \mathcal{D} = \frac{1}{4\alpha_0^3} + \mathfrak{E}, \mathfrak{E} \geq 0\}.$$

□

8. Drinking model by using Genocchi wavelet

The drinking dynamical model of arbitrary order formulated in the Caputo sense and solved using the Genocchi wavelet method. Here, the parameters are a=0.03, s=0.07, b=0.07, v=0.10 and the model is presented as follows:

$$^cD_0^\alpha S(\mathfrak{t}) = \Theta_1\Upsilon(\mathfrak{t}),$$

$$^cD_0^\alpha M(\mathfrak{t}) = \Theta_2\Upsilon(\mathfrak{t}),$$

$$^cD_0^\alpha R(\mathfrak{t}) = \Theta_3\Upsilon(\mathfrak{t}).$$

Here,

$$\Theta_1 = [\theta_1, \theta_2, \ldots, \theta_{\hat{m}}],$$

$$\Theta_2 = [\theta_{\hat{m}+1}, \theta_{\hat{m}+2}, \ldots, \theta_{2\hat{m}}],$$

$$\Theta_3 = [\theta_{2\hat{m}+1}, \theta_{2\hat{m}+2}, \ldots, \theta_{3\hat{m}}].$$

are the unknown vectors for the equations. Now, with the help of fractional integral operator and the initial condition we obtained

$$I_\mathfrak{t}^\alpha \, {}_0^C D_\mathfrak{t}^\alpha S(\mathfrak{t}) = S(\mathfrak{t}) - S(0) = \Theta_1\mathcal{P}^\alpha\Upsilon(\mathfrak{t}),$$

$$I_\mathfrak{t}^\alpha \, {}_0^C D_\mathfrak{t}^\alpha M(\mathfrak{t}) = M(\mathfrak{t}) - M(0) = \Theta_2\mathcal{P}^\alpha\Upsilon(\mathfrak{t}),$$

$$I_\mathfrak{t}^\alpha \, {}_0^C D_\mathfrak{t}^\alpha R(\mathfrak{t}) = R(\mathfrak{t}) - R(0) = \Theta_3\mathcal{P}^\alpha\Upsilon(\mathfrak{t}).$$

By using the above equations the fractional order drinking model can be rewritten like

$$\begin{aligned}
\Theta_1\Upsilon(\mathfrak{t}) &= -b\Big(\Theta_1\mathcal{P}^{\alpha}\Upsilon(\mathfrak{t})+\mathcal{I}\Big)\times\Big(\Theta_2\mathcal{P}^{\alpha}\Upsilon(\mathfrak{t})+\mathcal{J}\Big)-b\Big(\Theta_1\mathcal{P}^{\alpha}\Upsilon(\mathfrak{t})+\mathcal{I}\Big)\times\Big(\Theta_3\mathcal{P}^{\alpha}\Upsilon(\mathfrak{t})+\mathfrak{K}\Big)\\
&\quad+v\Big(\Theta_1\mathcal{P}^{\alpha}\Upsilon(\mathfrak{t})+\mathcal{I}\Big)\times\Big(\Theta_3\mathcal{P}^{\alpha}\Upsilon(\mathfrak{t})+\mathfrak{K}\Big),\\
\Theta_2\Upsilon(\mathfrak{t}) &= b\Big(\Theta_1\mathcal{P}^{\alpha}\Upsilon(\mathfrak{t})+\mathcal{I}\Big)\times\Big(\Theta_2\mathcal{P}^{\alpha}\Upsilon(\mathfrak{t})+\mathcal{J}\Big)+b\Big(\Theta_1\mathcal{P}^{\alpha}\Upsilon(\mathfrak{t})+\mathcal{I}\Big)\times\Big(\Theta_3\mathcal{P}^{\alpha}\Upsilon(\mathfrak{t})+\mathfrak{K}\Big)\\
&\quad-s\Big(\Theta_2\mathcal{P}^{\alpha}\Upsilon(\mathfrak{t})+\mathcal{J}\Big)\times\Big(\Theta_3\mathcal{P}^{\alpha}\Upsilon(\mathfrak{t})+\mathfrak{K}\Big)-a\Big(\Theta_2\mathcal{P}^{\alpha}\Upsilon(\mathfrak{t})+\mathcal{J}\Big),\\
\Theta_3\Upsilon(\mathfrak{t}) &= a\Big(\Theta_2\mathcal{P}^{\alpha}\Upsilon(\mathfrak{t})+\mathcal{J}\Big)+s\Big(\Theta_2\mathcal{P}^{\alpha}\Upsilon(\mathfrak{t})+\mathcal{J}\Big)\times\Big(\Theta_3\mathcal{P}^{\alpha}\Upsilon(\mathfrak{t})+\mathfrak{K}\Big)\\
&\quad-v\Big(\Theta_1\mathcal{P}^{\alpha}\Upsilon(\mathfrak{t})+\mathcal{I}\Big)\times\Big(\Theta_3\mathcal{P}^{\alpha}\Upsilon(\mathfrak{t})+\mathfrak{K}\Big).
\end{aligned}$$

By applying the collocation points, we get

$$\begin{aligned}
\Theta_1\Upsilon(\mathfrak{t}_{\mathfrak{i}}) &= -b\Big(\Theta_1\mathcal{P}^{\alpha}\Upsilon(\mathfrak{t}_{\mathfrak{i}})+\mathcal{I}\Big)\times\Big(\Theta_2\mathcal{P}^{\alpha}\Upsilon(\mathfrak{t})+\mathcal{J}\Big)-b\Big(\Theta_1\mathcal{P}^{\alpha}\Upsilon(\mathfrak{t}_{\mathfrak{i}})+\mathcal{I}\Big)\times\Big(\Theta_3\mathcal{P}^{\alpha}\Upsilon(\mathfrak{t}_{\mathfrak{i}})+\mathfrak{K}\Big)\\
&\quad+v\Big(\Theta_1\mathcal{P}^{\alpha}\Upsilon(\mathfrak{t}_{\mathfrak{i}})+\mathcal{I}\Big)\times\Big(\Theta_3\mathcal{P}^{\alpha}\Upsilon(\mathfrak{t}_{\mathfrak{i}})+\mathfrak{K}\Big),\\
\Theta_2\Upsilon(\mathfrak{t}_{\mathfrak{i}}) &= b\Big(\Theta_1\mathcal{P}^{\alpha}\Upsilon(\mathfrak{t}_{\mathfrak{i}})+\mathcal{I}\Big)\times\Big(\Theta_2\mathcal{P}^{\alpha}\Upsilon(\mathfrak{t}_{\mathfrak{i}})+\mathcal{J}\Big)+b\Big(\Theta_1\mathcal{P}^{\alpha}\Upsilon(\mathfrak{t}_{\mathfrak{i}})+\mathcal{I}\Big)\times\Big(\Theta_3\mathcal{P}^{\alpha}\Upsilon(\mathfrak{t}_{\mathfrak{i}})+\mathfrak{K}\Big)\\
&\quad-s\Big(\Theta_2\mathcal{P}^{\alpha}\Upsilon(\mathfrak{t}_{\mathfrak{i}})+\mathcal{J}\Big)\times\Big(\Theta_3\mathcal{P}^{\alpha}\Upsilon(\mathfrak{t}_{\mathfrak{i}})+\mathfrak{K}\Big)-a\Big(\Theta_2\mathcal{P}^{\alpha}\Upsilon(\mathfrak{t}_{\mathfrak{i}})+\mathcal{J}\Big),\\
\Theta_3\Upsilon(\mathfrak{t}_{\mathfrak{i}}) &= a\Big(\Theta_2\mathcal{P}^{\alpha}\Upsilon(\mathfrak{t}_{\mathfrak{i}})+\mathcal{J}\Big)+s\Big(\Theta_2\mathcal{P}^{\alpha}\Upsilon(\mathfrak{t}_{\mathfrak{i}})+\mathcal{J}\Big)\times\Big(\Theta_3\mathcal{P}^{\alpha}\Upsilon(\mathfrak{t}_{\mathfrak{i}})+\mathfrak{K}\Big)\\
&\quad-v\Big(\Theta_1\mathcal{P}^{\alpha}\Upsilon(\mathfrak{t}_{\mathfrak{i}})+\mathcal{I}\Big)\times\Big(\Theta_3\mathcal{P}^{\alpha}\Upsilon(\mathfrak{t}_{\mathfrak{i}})+\mathfrak{K}\Big).
\end{aligned}$$

By addressing the given set of algebraic equations using MATLAB, we will obtain the solutions for $3\hat{m}$ number of unknowns.

9. Adams Bashforth Moulton Technique

In this subsection, we will apply ABM technique to solve the drinking behavior dynamical model of arbitrary order as follows [12, 13]

$$\begin{aligned}
S_{m+1} &= \mathcal{I}+\frac{\mathfrak{h}^{\alpha}}{\Gamma(\alpha+2)}\Big(-b(\mathfrak{t}_{\mathfrak{m}+1})S^{\mathcal{P}}_{m+1}M^{\mathcal{P}}_{m+1}-b(\mathfrak{t}_{\mathfrak{m}+1})S^{\mathcal{P}}_{m+1}R^{\mathcal{P}}_{m+1}+v(\mathfrak{t}_{\mathfrak{m}+1})S^{\mathcal{P}}_{m+1}R^{\mathcal{P}}_{m+1}\Big)\\
&\quad+\frac{\mathfrak{h}^{\alpha}}{\Gamma(\alpha+2)}\sum_{J=0}^{m}A_{J,m+1}\Big(-b(\mathfrak{t}_J)S_JM_J-b(\mathfrak{t}_J)S_JR_J+v(\mathfrak{t}_J)S_JR_J\Big),\\
M_{m+1} &= \mathcal{J}+\frac{\mathfrak{h}^{\alpha}}{\Gamma(\alpha+2)}\Big(b(\mathfrak{t}_{\mathfrak{m}+1})S^{\mathcal{P}}_{m+1}M^{\mathcal{P}}_{m+1}+b(\mathfrak{t}_{\mathfrak{m}+1})S^{\mathcal{P}}_{m+1}R^{\mathcal{P}}_{m+1}\\
&\quad-s(\mathfrak{t}_{\mathfrak{m}+1})M^{\mathcal{P}}_{m+1}R^{\mathcal{P}}_{m+1}-a(\mathfrak{t}_{\mathfrak{m}+1})M^{\mathcal{P}}_{m+1}\Big)\\
&\quad+\frac{\mathfrak{h}^{\alpha}}{\Gamma(\alpha+2)}\sum_{J=0}^{m}A_{J,m+1}\Big(b(\mathfrak{t}_J)S_JM_J+b(\mathfrak{t}_J)S_JR_J-s(\mathfrak{t}_J)M_JR_J-a(\mathfrak{t}_J)M_J\Big),\\
R_{m+1} &= \mathfrak{K}+\frac{\mathfrak{h}^{\alpha}}{\Gamma(\alpha+2)}\Big(a(\mathfrak{t}_{\mathfrak{m}+1})M^{\mathcal{P}}_{m+1}+s(\mathfrak{t}_{\mathfrak{m}+1})M^{\mathcal{P}}_{m+1}R^{\mathcal{P}}_{m+1}\\
&\quad-v(\mathfrak{t}_{\mathfrak{m}+1})S^{\mathcal{P}}_{m+1}R^{\mathcal{P}}_{m+1}\Big)\\
&\quad+\frac{\mathfrak{h}^{\alpha}}{\Gamma(\alpha+2)}\sum_{J=0}^{m}A_{J,m+1}\Big(a(\mathfrak{t}_J)M_J+s(\mathfrak{t}_J)M_JR_J-v(\mathfrak{t}_J)S_JR_J\Big).
\end{aligned}$$

Where,

$$S_{m+1} = \mathcal{I} + \frac{1}{\Gamma(\alpha)} \sum_{J=0}^{m} B_{J,m+1}\Big(- b(\mathfrak{t}_J) S_J M_J - b(\mathfrak{t}_J) S_J R_J + v(\mathfrak{t}_J) S_J R_J \Big),$$

$$M_{m+1} = \mathcal{J} + \frac{1}{\Gamma(\alpha)} \sum_{J=0}^{m} B_{J,m+1}\Big(b(\mathfrak{t}_J) S_J M_J + b(\mathfrak{t}_J) S_J R_J - s(\mathfrak{t}_J) M_J R_J - a(\mathfrak{t}_J) M_J \Big),$$

$$R_{m+1} = \mathfrak{K} + \frac{1}{\Gamma(\alpha)} \sum_{J=0}^{m} B_{J,m+1}\Big(a(\mathfrak{t}_J) M_J + s(\mathfrak{t}_J) M_J R_J - v(\mathfrak{t}_J) S_J R_J \Big).$$

$A_{J_0,m+1} =$

$$\begin{cases} -(m-\alpha) \times (m+1) + m^{\alpha+1} \text{ if } J_0 = 0, \\ \\ -(-(m-J_0)^{\alpha+1} + 2(m-J_0+1)^{\alpha+1}) + (m-J_0+2)^{\alpha+1} \text{ if } 1 \le J_0 \le m, \\ 1 \text{ if } J_0 = m+1. \end{cases}$$

$$B_{J_0,m+1} = \frac{\mathfrak{h}^{\alpha}}{\alpha}(-(m-J_0)^{\alpha} + (m-J_0+1)^{\alpha}),\ 0 \le J_0 \le m.$$

10. Numerical discussion

Fig. 1 illustrates the behavior of the susceptible population (S) over time, showing a steady decline as individuals transition to moderate or risk drinking categories due to interactions and probabilities of influence. Fig. 2 represents the moderate drinkers (M) population, which initially rises as susceptible individuals join the category and then gradually declines as moderate drinkers transition to risk drinkers or quit drinking. Fig. 3 shows the risk drinkers (R) population, which displays a consistent increase over time and reflecting the accumulation of individuals transitioning from moderate drinking due to stress, depression or influence from other risk drinkers. Fig. 4 compares the behavior of the S for varying non integer orders α and demonstrating smoother transitions and memory effects at different α values that highlighting how fractional order influences system dynamics. In Fig. 5, the M is analyzed under various α values, showing more gradual transitions for lower α, emphasizing the long-term memory effect. Fig. 6 examines the behavior of R under different α values, where higher fractional orders result in steeper transitions and quicker stabilization of the risk drinker population. Fig. 7 provides a 3D representation of S population dynamics, showcasing the influence of time and fractional order, with a non-linear decrease in the susceptible category. Fig. 8 presents a 3D plot of M, illustrating the combined effect of time and fractional order, showing growth and eventual decline depending on α. Fig. 9 depicts the 3D dynamics of R, demonstrating a consistent rise across time and fractional orders, with the influence of α evident in the slope and stabilization behavior. Figs. 10, 11, and 12 compare the system categories as SM, MR, RP at $\alpha = 0.98$ respectively. Fig. 13 shows the system behavior at $\alpha = 1$, representing integer-order dynamics with sharp transitions among categories. In Fig. 14, mentions the susceptible and moderate for $\alpha = 0.9$. Fig. 15 validates the model results for $\alpha = 0.9$, showing responses in moderate and risk drinkers. Fig. 16 summarizes the results at $\alpha = 0.9$, confirming risk drinkers to susceptible. At $\alpha = 1.0$, Fig. 17 highlights faster transitions and sharper behavior of S and M. Fig. 18 corroborates the classical approach for $\alpha = 1.0$, for M and R. Fig. 19 summarizes the results for $\alpha = 1.0$, for R and P highlighting the limitations of integer-order modeling in representing smooth and realistic dynamics. Fig. 20 provides an error analysis

for the S, demonstrating the accuracy of the Genocchi wavelet method with minimal errors across time. Fig. 21 confirms the reliability of the proposed method through error analysis for Moderate drinkers M, with consistently low errors showcasing the method?s precision. Finally, Fig. 22 presents the error analysis for Risk drinkers R, indicating high accuracy and validating the method's applicability for non-linear systems modeling. Fig. 23 showcases the comparison of the susceptible drinkers population by utilizing GWM and ABM. Both methods produce similar results, indicating a close agreement between GWM and ABM in modeling the dynamics of the susceptible drinkers population. Fig. 24 shows the comparison of the moderate drinkers population by utilizing GWM and ABM. This also shows a similar outcomes. Fig. 25 illustrates the comparison of the risk drinkers population by utilizing GWM and ABM. This also produces a same results. Fig. 26 compares three methods for solving $S(t)$ over time t. The BW and ABM methods closely align and the previous method deviates slightly particularly in the mid-range values of t. Fig. 27 shows the results of three methods for solving $M(t)$. The BW, and the ABM, closely align but the previous method deviates when going to the peak. Fig. 28 presents a comparison of three methods BW, ABM and a previous method for solving $R(t)$ over time t. The BW and ABM methods closely align and shows higher accuracy compared to the previous method which deviates significantly. Figs. 29-31 are 3D plots that illustrate the variation of the functions with respect to t and different ranges of α. The surface shows a influence of α on the function's behavior. The values represent computed results of a model, likely showing how the error values varies with changes in α. 36 shows that the model output closely aligns with the real data on alcohol consumption in Brunei (2000-2020), especially for $\alpha = 0.995$. The x-axis values are scaled using a factor of 0.105, such that the time domain [0, 200] corresponds to the years 2000-2020. Table 2, 3, and 4 mention the absolute error values of the S, M, and R respectively by utilizing GWM and ABM. Tables 5-6 mention the absolute error values of the S, M, and R respectively by utilizing GWM and ABM for different values of α. These table presents numerical results for different values of t and fractional order α ranging from 0.7 to 1. Now, GW has slightly more accurate results (with lower absolute error) compared to ABM in the table 8. In Table 9 GW has lower AE in 9 out of 11 cases. In Table 10 , the GW method clearly provides better accuracy than ABM at every single time value.

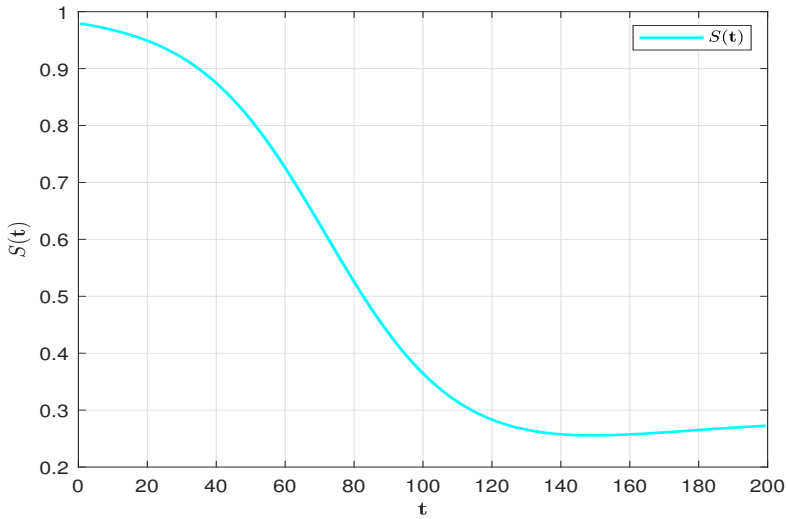

Figure 1: Behavior of susceptible population.

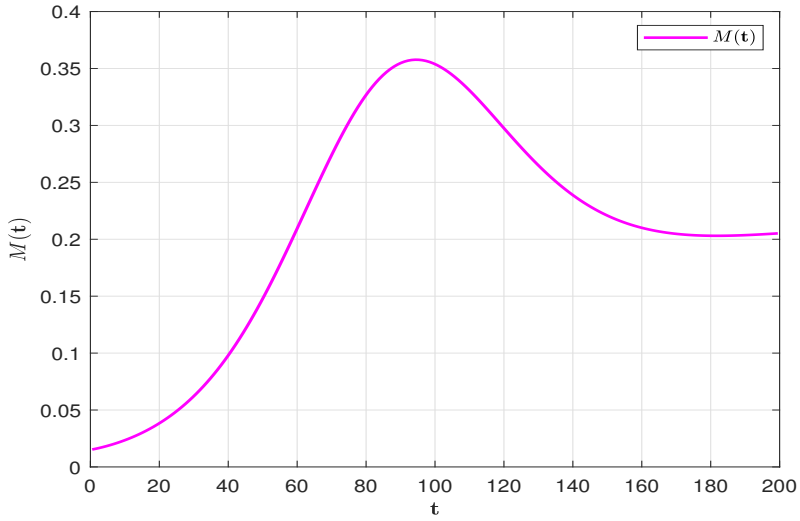

Figure 2: Behavior of moderate population.

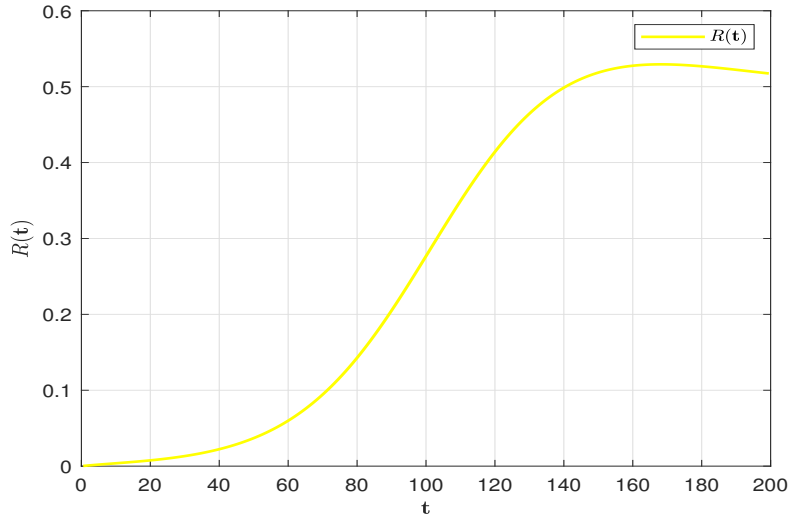

Figure 3: Behavior of risk population.

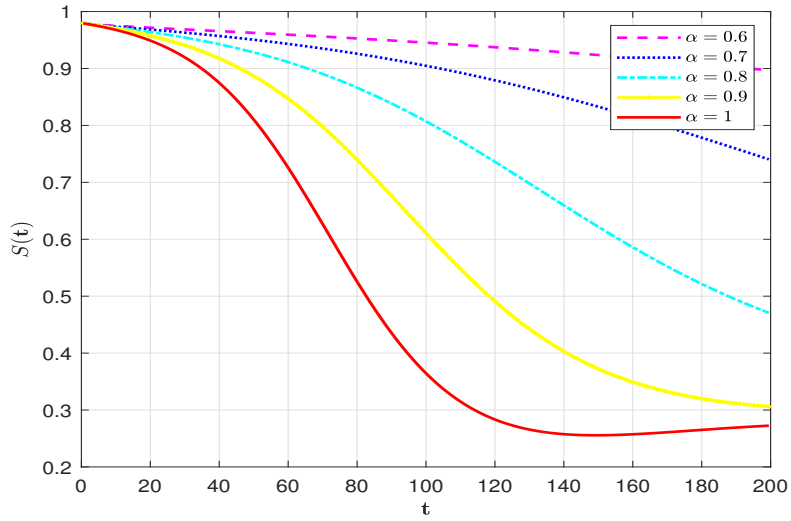

Figure 4: Behavior of susceptible population at various α values at 192.

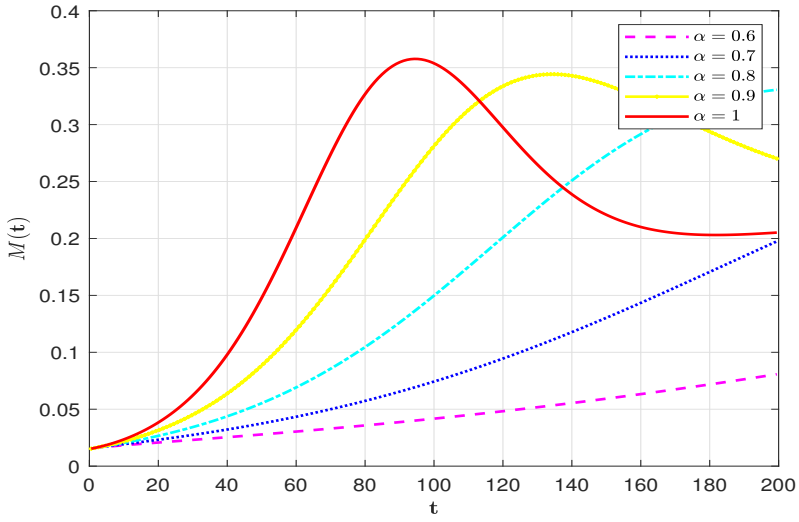

Figure 5: Behavior of moderate population at various α values at $\hat{m} = 192$.

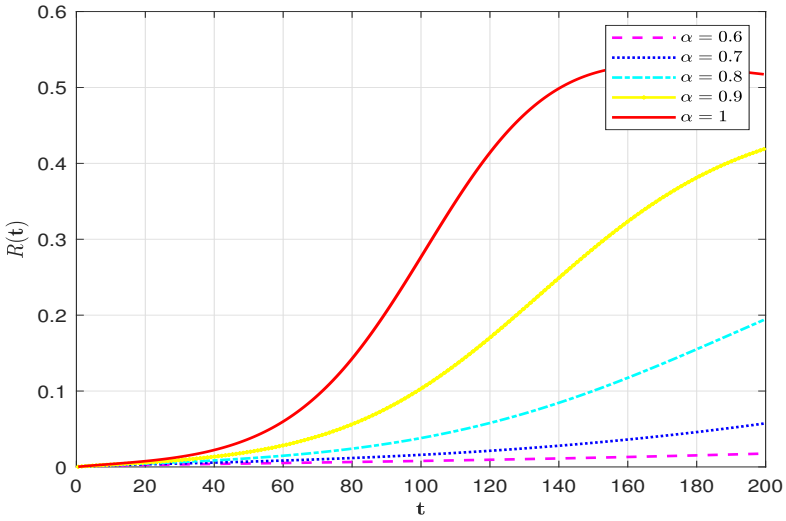

Figure 6: Behavior of risk population at various α values at 192.

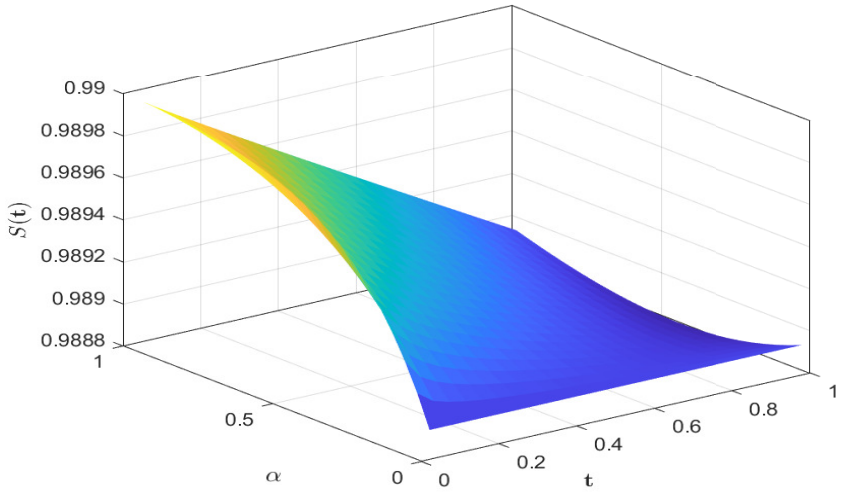

Figure 7: 3D Representation of susceptible population.

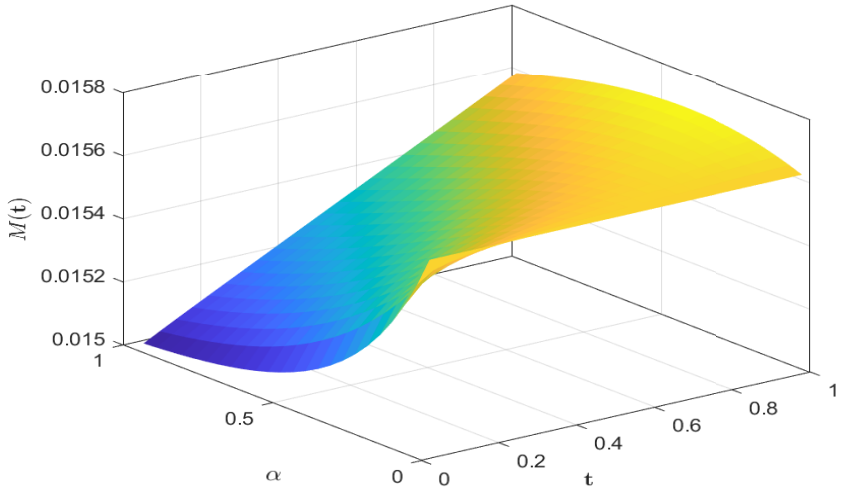

Figure 8: 3D Representation of moderate population.

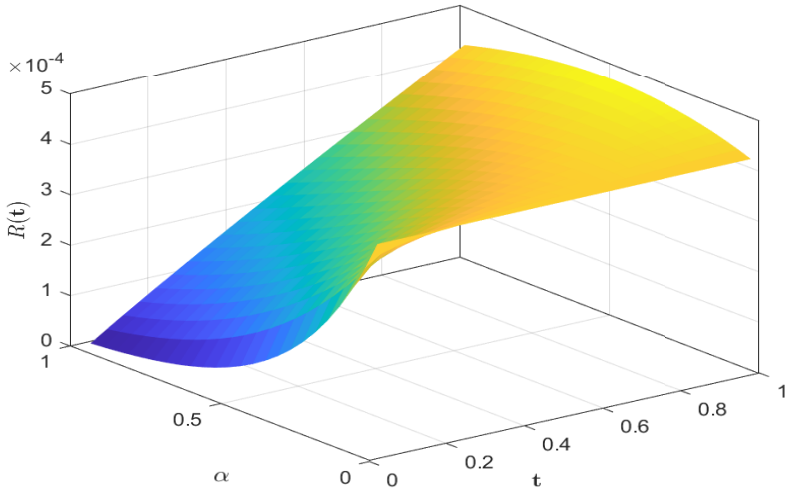

Figure 9: 3D Representation of risk population.

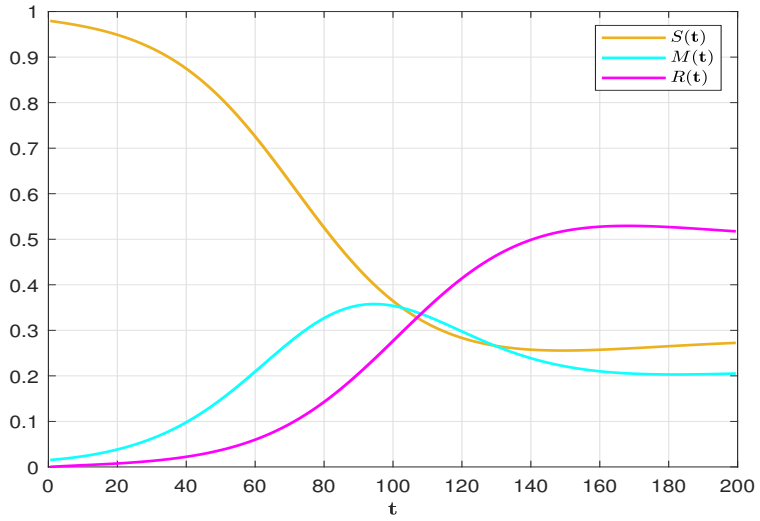

Figure 10: System Behavior at $\alpha = 1$.

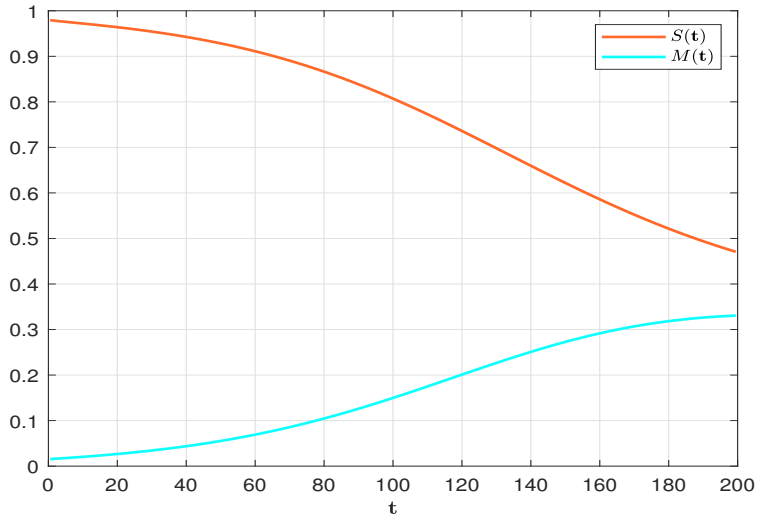

Figure 11: SM at $\alpha = 0.8$.

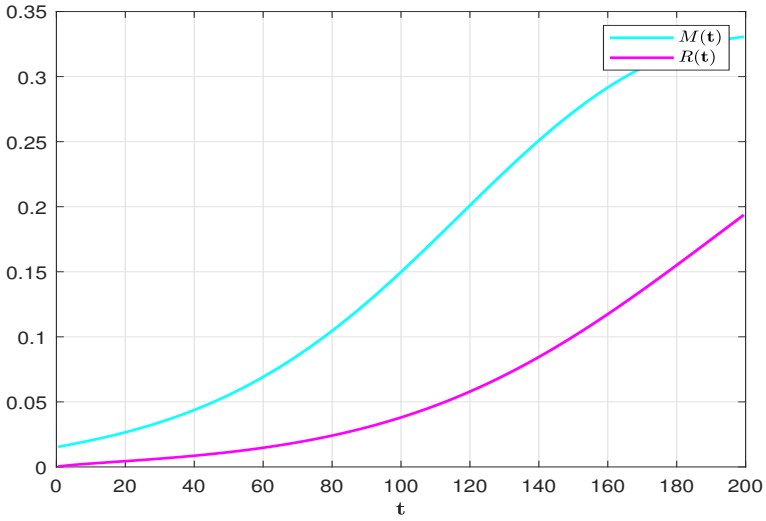

Figure 12: MR at $\alpha = 0.8$.

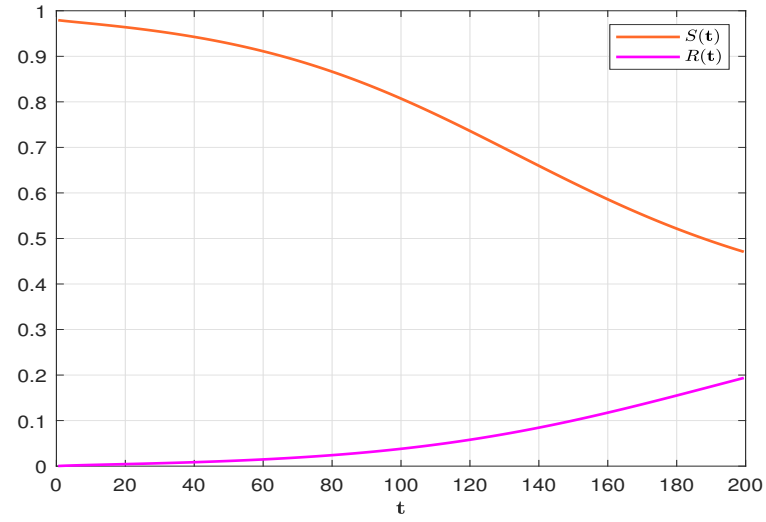

Figure 13: RS at $\alpha = 0.8$.

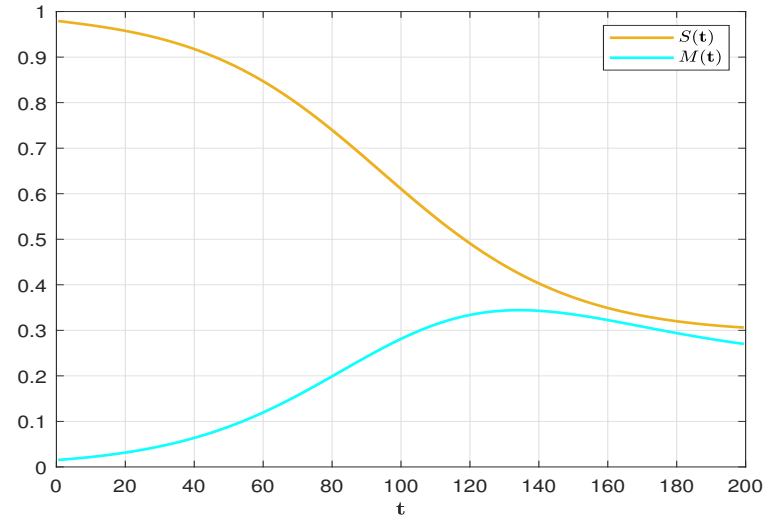

Figure 14: SM for $\alpha = 0.9$.

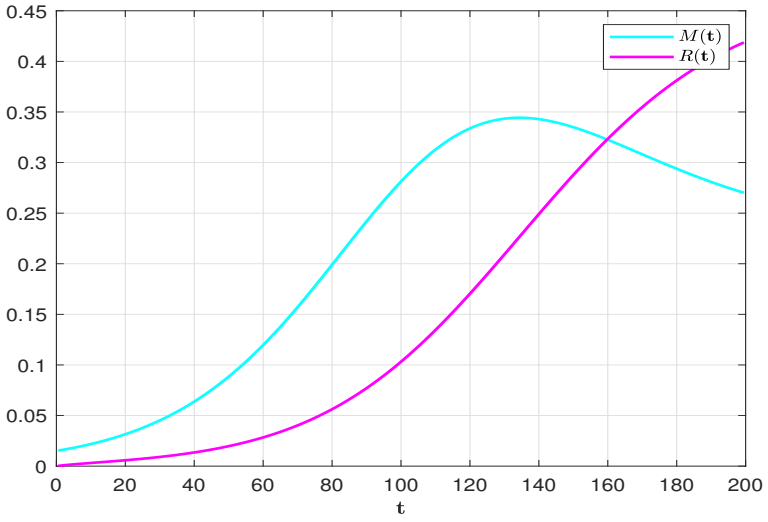

Figure 15: Model Results (MR) for $\alpha = 0.9$.

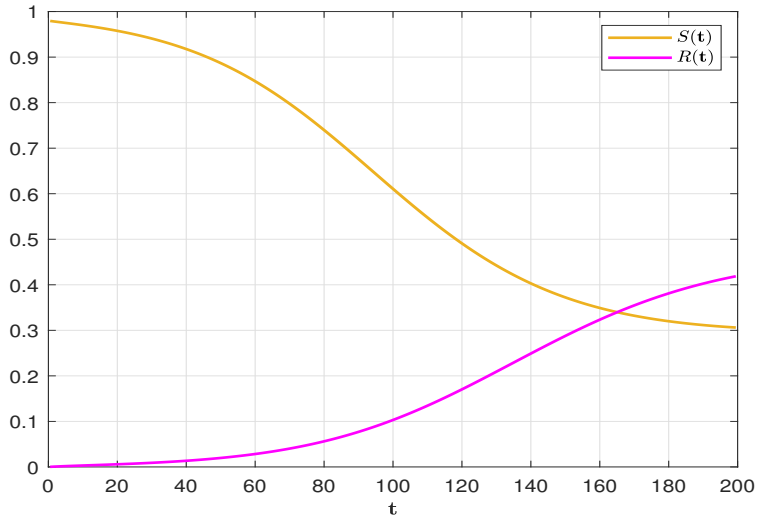

Figure 16: RS for $\alpha = 0.9$.

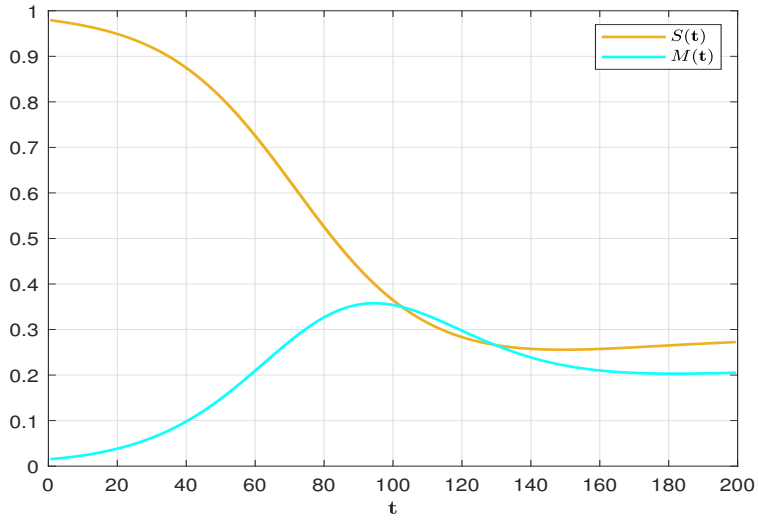

Figure 17: SM for $\alpha = 1$.

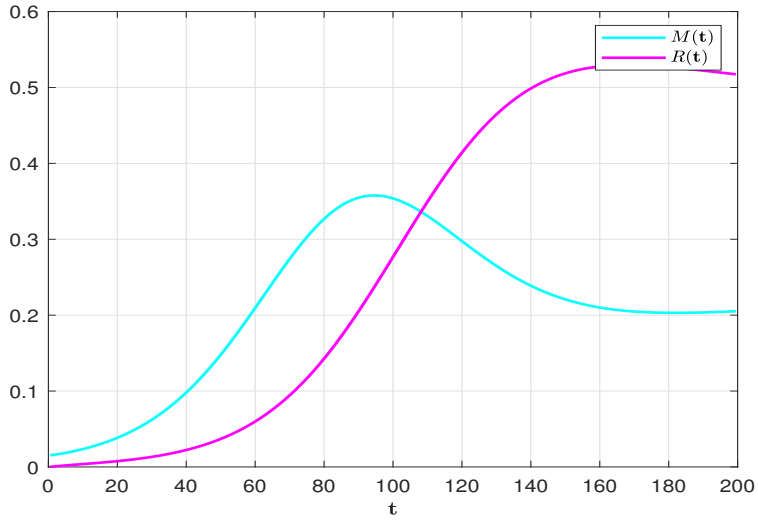

Figure 18: MR for $\alpha = 1$.

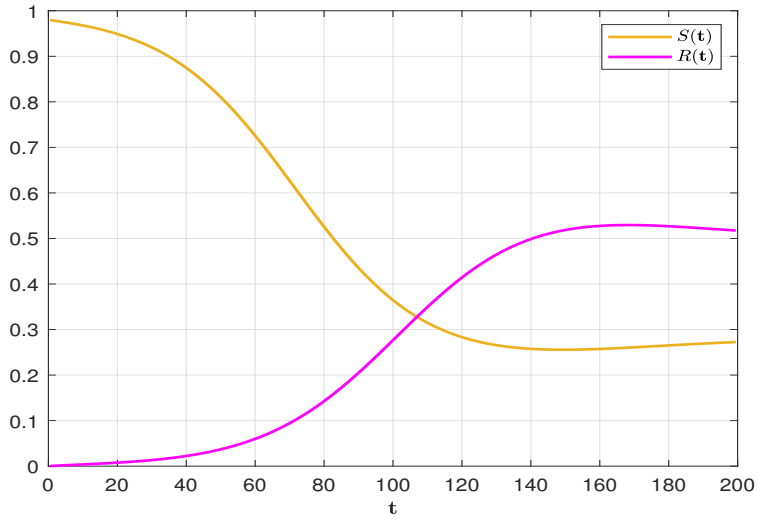

Figure 19: RS for $\alpha = 1$.

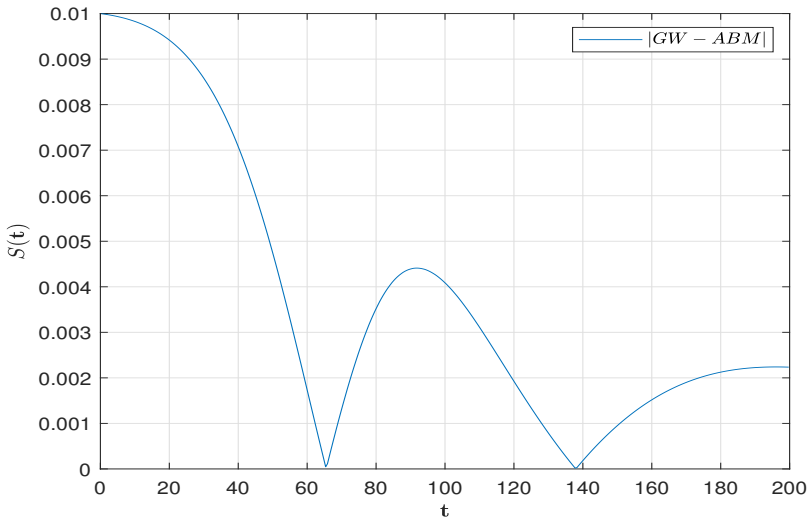

Figure 20: Absolute error values for S(t).

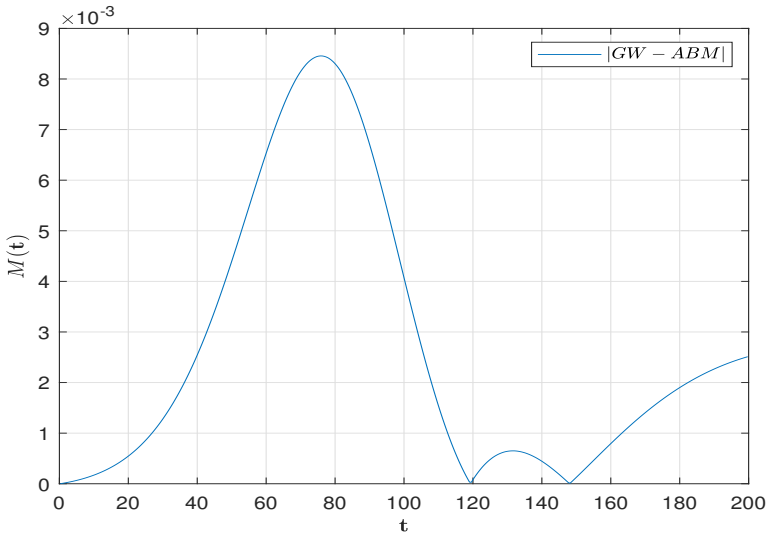

Figure 21: Absolute error values for M(t).

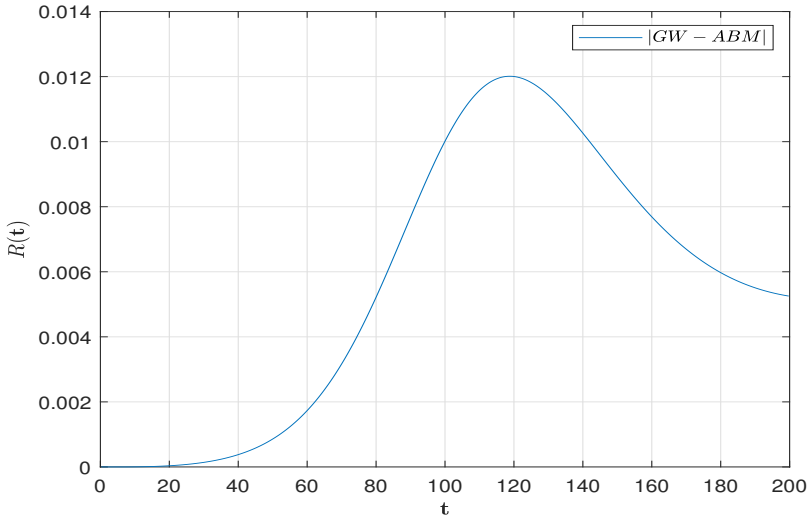

Figure 22: Absolute error values for R(t).

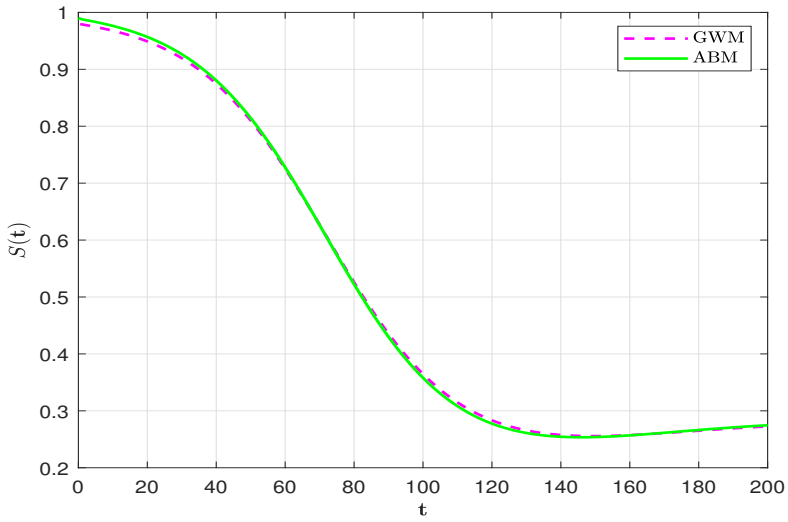

Figure 23: Comparison of susceptible drinkers population by using GWM and ABM

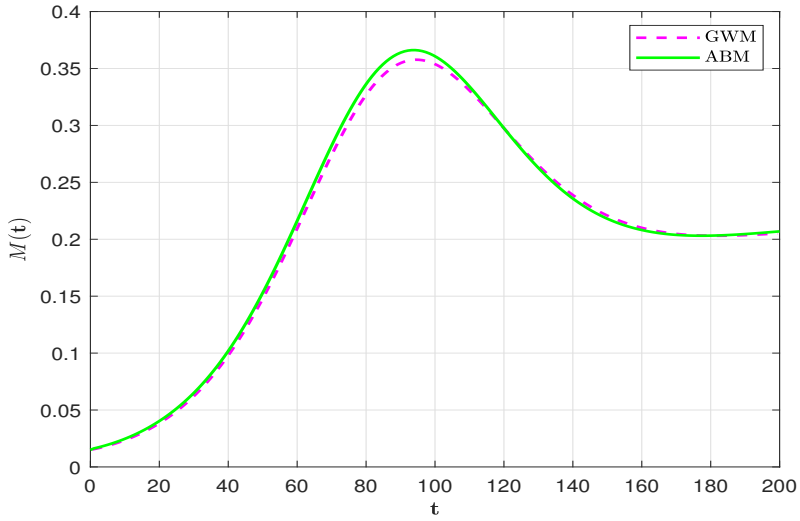

Figure 24: Comparison of moderate drinkers population by using GWM and ABM.

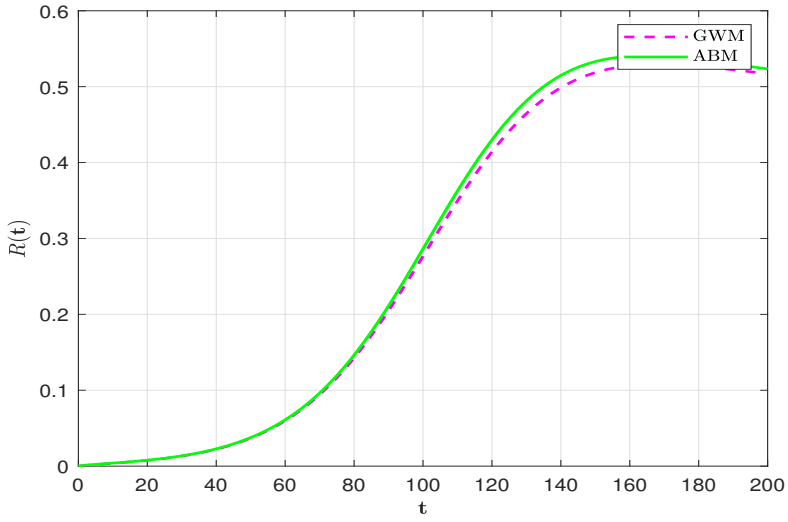

Figure 25: Comparison of risk drinkers population by using GWM and ABM.

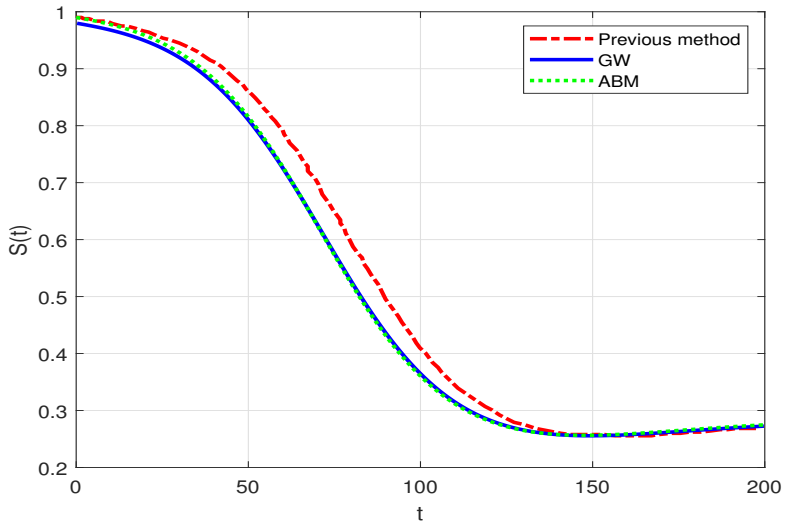

Figure 26: Comparison of GW, ABM, and previous methods for $S(t)$.

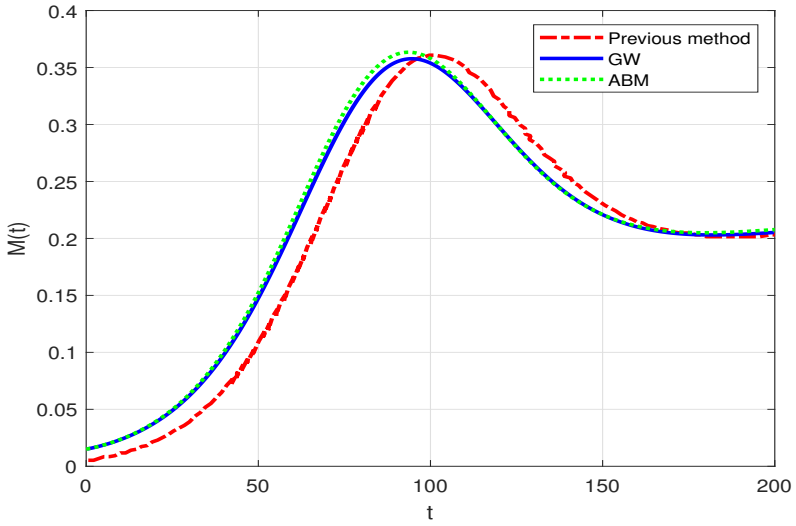

Figure 27: Comparison of GW, ABM, and previous methods for $M(t)$.

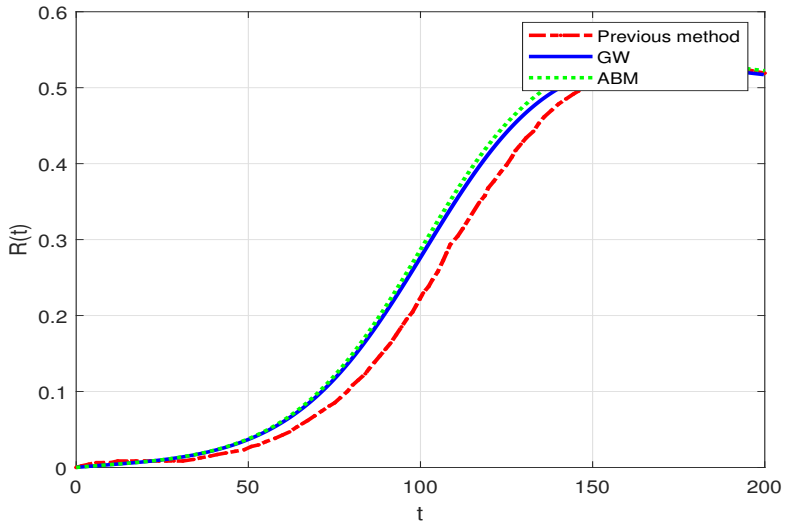

Figure 28: Comparison of GW, ABM, and previous methods for $R(t)$.

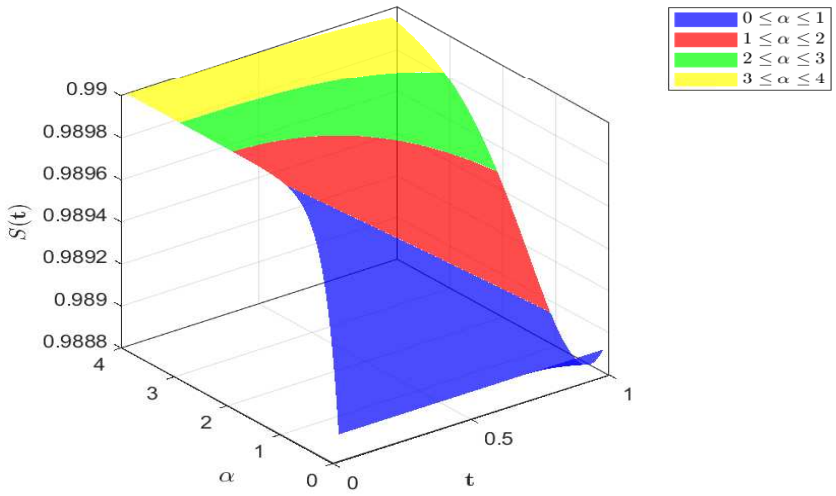

Figure 29: Different ranges of α for $S(t)$ in 3D.

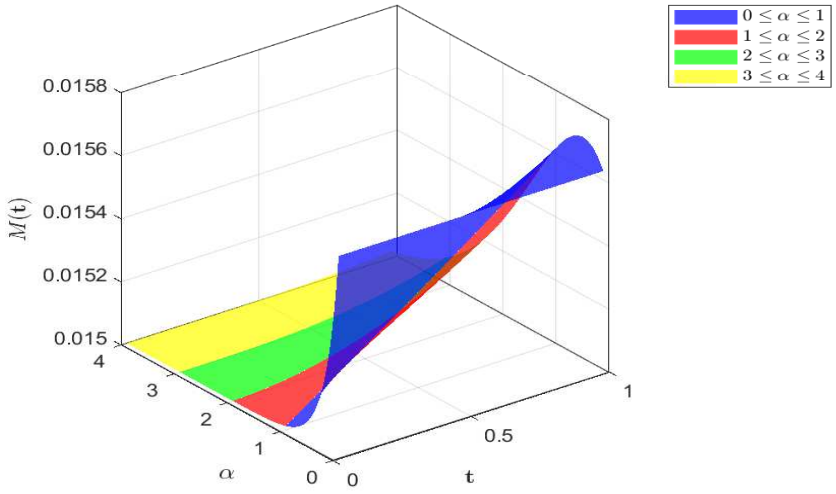

Figure 30: Different ranges of α for $M(t)$ in 3D.

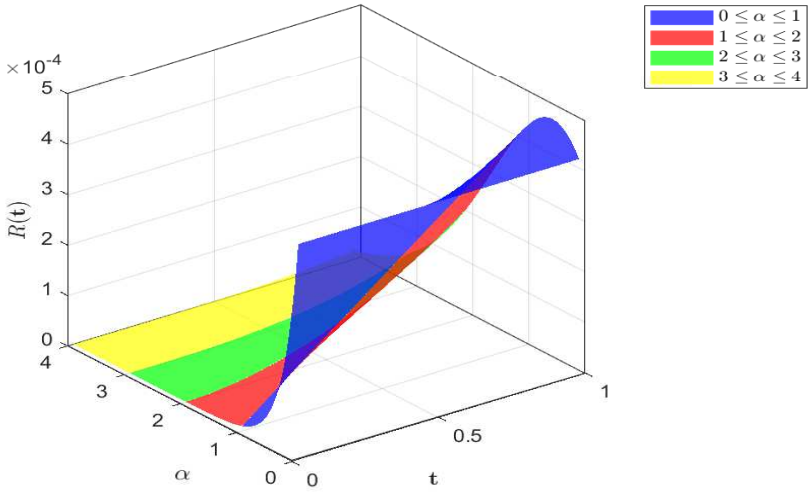

Figure 31: Different ranges of α for $R(t)$ in 3D.

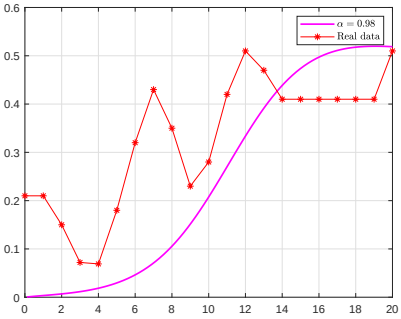

Figure 32: Real data vs $\alpha = 0.98$.

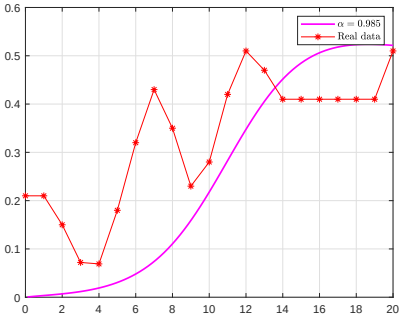

Figure 33: Real data vs $\alpha = 0.985$.

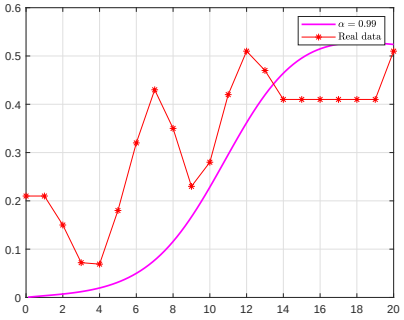

Figure 34: Real data vs $\alpha = 0.99$.

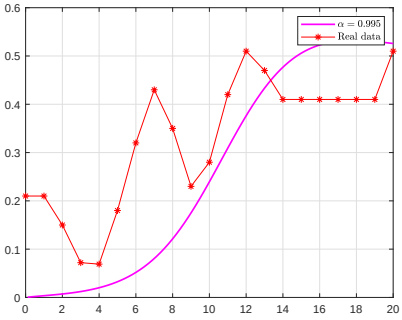

Figure 35: Real data vs $\alpha = 0.995$.

Figure 36: The drinking population at different fractional orders along with real data.

Table 1: Model parameter values

Parameter	**Value**
b	0.07
s	0.07
v	0.10
a	0.03

Table 2: Comparison of ABM, GW, and Absolute Error for given $\mathfrak{t}$ values.

$\mathfrak{t}$	ABM	GW	Absolute Error
0.2	0.989728197189743	0.979730233368269	9.998×10^{-3}
1.3	0.988622396381879	0.978635907243232	9.9865×10^{-3}
2.3	0.987481711962011	0.977508166634674	9.9735×10^{-3}
3.3	0.986301896452239	0.976342462252051	9.9594×10^{-3}
4.4	0.985078143881175	0.975134341240092	9.9438×10^{-3}
5.4	0.983805680373291	0.973879419789057	9.9263×10^{-3}

Table 3: Comparison of ABM, GW, and Absolute Error for various $\mathfrak{t}$ values.

$\mathfrak{t}$	ABM	GW	Absolute Error
0.2	0.0151554164102500	0.0151542881504388	1.1283×10^{-6}
1.3	0.0158124578356750	0.0157995183949071	1.2939×10^{-5}
2.3	0.0165272668972457	0.0165011080272182	2.6159×10^{-5}
3.3	0.0173001675262914	0.0172595817150001	4.0586×10^{-5}
4.4	0.0181321674525307	0.0180757325404941	5.6435×10^{-5}
5.4	0.0190245796024014	0.0189506043015756	7.3975×10^{-5}

Table 4: Comparison of ABM, GW, and Absolute Error for different $\mathfrak{t}$ values.

$\mathfrak{t}$	ABM	GW	Absolute Error
0.2	0.000116386400006766	0.000115478481292510	9.0792×10^{-7}
1.3	0.000565145782445893	0.000564574361861450	5.7142×10^{-7}
2.3	0.000991021140743874	0.000990725338107595	2.9580×10^{-7}
3.3	0.00139793602147010	0.00139795603294858	2.0011×10^{-8}
4.4	0.00178968866629435	0.00178992621941413	2.3755×10^{-7}
5.4	0.00216974002430809	0.00216997590936704	2.3589×10^{-7}

Table 5: Absolute error of $S(t)$ for different values of α.

t	$\alpha = 0.7$	$\alpha = 0.8$	$\alpha = 0.9$	$\alpha = 1$
0.2604	1.8642×10^{-5}	1.1366×10^{-5}	4.8161×10^{-6}	9.9980×10^{-3}
20.0521	7.4604×10^{-7}	1.3303×10^{-6}	2.9248×10^{-6}	9.4149×10^{-3}
40.3646	1.7597×10^{-6}	2.8893×10^{-6}	6.9831×10^{-6}	7.0076×10^{-3}
60.1563	3.4797×10^{-6}	5.6823×10^{-6}	1.3260×10^{-5}	1.6849×10^{-3}
80.4688	6.0823×10^{-6}	9.6706×10^{-6}	1.8062×10^{-5}	3.5909×10^{-3}
100.2604	9.1756×10^{-6}	1.2904×10^{-5}	1.5206×10^{-5}	4.0685×10^{-3}
120.0521	1.3162×10^{-5}	1.5341×10^{-5}	1.0190×10^{-5}	1.9185×10^{-3}
140.3646	1.7700×10^{-5}	1.5509×10^{-5}	5.9816×10^{-6}	2.1422×10^{-4}
160.1563	2.1950×10^{-5}	1.3349×10^{-5}	3.4958×10^{-6}	1.5246×10^{-3}
180.4688	2.5233×10^{-5}	9.5201×10^{-6}	1.9094×10^{-6}	2.1327×10^{-3}
199.7396	2.7399×10^{-5}	6.3780×10^{-6}	1.1418×10^{-6}	2.2354×10^{-3}

Table 6: Absolute error of $M(t)$ for different values of α.

t	$\alpha = 0.7$	$\alpha = 0.8$	$\alpha = 0.9$	$\alpha = 1$
0.2604	5.0089×10^{-3}	5.0049×10^{-3}	5.0013×10^{-3}	1.1283×10^{-6}
20.0521	4.9995×10^{-3}	4.9990×10^{-3}	4.9977×10^{-3}	5.4888×10^{-4}
40.3646	4.9988×10^{-3}	4.9978×10^{-3}	4.9945×10^{-3}	2.6012×10^{-3}
60.1563	4.9974×10^{-3}	4.9956×10^{-3}	4.9900×10^{-3}	6.5646×10^{-3}
80.4688	4.9954×10^{-3}	4.9927×10^{-3}	4.9880×10^{-3}	8.2641×10^{-3}
100.2604	4.9930×10^{-3}	4.9907×10^{-3}	4.9928×10^{-3}	3.9999×10^{-3}
120.0521	4.9901×10^{-3}	4.9900×10^{-3}	4.9985×10^{-3}	8.4866×10^{-5}
140.3646	4.9869×10^{-3}	4.9915×10^{-3}	5.0017×10^{-3}	4.2829×10^{-4}
160.1563	4.9842×10^{-3}	4.9948×10^{-3}	5.0024×10^{-3}	8.0345×10^{-4}
180.4688	4.9826×10^{-3}	4.9985×10^{-3}	5.0020×10^{-3}	1.9206×10^{-3}
199.7396	4.9822×10^{-3}	5.0010×10^{-3}	5.0017×10^{-3}	2.5110×10^{-3}

Table 7: Absolute error of $R(t)$ for different values of α.

t	$\alpha = 0.7$	$\alpha = 0.8$	$\alpha = 0.9$	$\alpha = 1$
0.2604	9.71×10^{-6}	6.52×10^{-6}	3.53×10^{-6}	9.08×10^{-7}
20.0521	2.48×10^{-7}	3.03×10^{-7}	5.76×10^{-7}	3.63×10^{-5}
40.3646	5.19×10^{-7}	6.54×10^{-7}	1.46×10^{-6}	3.91×10^{-4}
60.1563	8.99×10^{-7}	1.28×10^{-6}	3.26×10^{-6}	1.75×10^{-3}
80.4688	1.47×10^{-6}	2.35×10^{-6}	6.09×10^{-6}	5.33×10^{-3}
100.2604	2.19×10^{-6}	3.65×10^{-6}	8.04×10^{-6}	1.01×10^{-2}
120.0521	3.22×10^{-6}	5.33×10^{-6}	8.73×10^{-6}	1.20×10^{-2}
140.3646	4.57×10^{-6}	7.03×10^{-6}	7.72×10^{-6}	1.02×10^{-2}
160.1563	6.14×10^{-6}	8.13×10^{-6}	5.93×10^{-6}	7.67×10^{-3}
180.4688	7.84×10^{-6}	8.03×10^{-6}	3.92×10^{-6}	5.95×10^{-3}
199.7396	9.56×10^{-6}	7.34×10^{-6}	2.81×10^{-6}	5.25×10^{-3}

Table 8: Comparison of solutions of $S(t)$ with different methods

t	S (GW)	S (ABM)	S [10]	AE (GW vs [10])	AE (ABM vs [10])
0.2	0.979730233368	0.979735311571	0.997830802603	1.81006×10^{-2}	1.80955×10^{-2}
20	0.948937883752	0.948937381171	0.947939262472	9.98621×10^{-4}	9.98119×10^{-4}
40	0.869902693252	0.869906393148	0.869848156182	5.45371×10^{-5}	5.82370×10^{-5}
60	0.724336509920	0.724343308209	0.724511930585	1.75421×10^{-4}	1.68622×10^{-4}
80	0.521016536635	0.521019887382	0.520607375271	4.09161×10^{-4}	4.12512×10^{-4}
100	0.362976971212	0.362947961303	0.362255965292	7.21006×10^{-4}	6.91996×10^{-4}
120	0.283229654505	0.283240446663	0.284164859002	9.35204×10^{-4}	9.24412×10^{-4}
140	0.257407804280	0.257405607492	0.258134490238	7.26686×10^{-4}	7.28883×10^{-4}
160	0.257558345048	0.257558007586	0.258134490238	5.76145×10^{-4}	5.76483×10^{-4}
180	0.265303060988	0.265306393223	0.264642082429	6.60979×10^{-4}	6.64311×10^{-4}
199	0.272545349721	0.272546677645	0.271149674620	1.39568×10^{-3}	1.39700×10^{-3}

Table 9: Comparison of solutions of $M(t)$ with different methods

t	M (GW)	M (ABM)	M [10]	AE (GW vs [10])	AE (ABM vs [10])
0.2	0.01515428815	0.02201587289	0.01515151515	2.7730×10^{-6}	6.8644×10^{-3}
20	0.03843509705	0.04661844603	0.03896103896	5.2594×10^{-4}	7.6574×10^{-3}
40	0.10177721823	0.10989011035	0.10173160173	4.5617×10^{-5}	8.1585×10^{-3}
60	0.21040320530	0.21813332271	0.21861471861	8.2115×10^{-3}	4.8139×10^{-4}
80	0.32869022662	0.33548285619	0.32900432900	3.1410×10^{-4}	6.4785×10^{-3}
100	0.35348905142	0.35860129237	0.35930735930	5.8183×10^{-3}	7.0607×10^{-4}
120	0.29737834028	0.30025380777	0.29437229437	3.0060×10^{-3}	5.8815×10^{-3}
140	0.23799903178	0.23617358424	0.23809523809	9.6206×10^{-5}	1.9217×10^{-3}
160	0.20956539490	0.21459503399	0.20995670995	3.9132×10^{-4}	4.6383×10^{-3}
180	0.20307045989	0.20516909931	0.20346320346	3.9274×10^{-4}	1.7059×10^{-3}
199	0.20522076986	0.20640243581	0.20562770562	4.0694×10^{-4}	7.7473×10^{-4}

Table 10: Comparison of solutions of $R(t)$ with different methods

t	R (GW)	R (ABM)	R [10]	AE (GW vs [10])	AE (ABM vs [10])
0.2	0.000115478481	0.003248815531	0	1.154785×10^{-4}	3.248816×10^{-3}
20	0.007627019191	0.009444172790	0.010822511000	7.627019×10^{-3}	9.444173×10^{-3}
40	0.023320088510	0.025203496499	0.023809524000	2.332009×10^{-2}	2.520350×10^{-2}
60	0.060260284778	0.062523369077	0.060606061000	6.026028×10^{-2}	6.252337×10^{-2}
80	0.145293236743	0.148497256419	0.145021645000	1.452932×10^{-1}	1.484973×10^{-1}
100	0.278533977364	0.283450746321	0.277056277000	2.785340×10^{-1}	2.834507×10^{-1}
120	0.414392005206	0.421505745563	0.415584416000	4.143920×10^{-1}	4.215057×10^{-1}
140	0.499593163934	0.511420808267	0.497835498000	4.995932×10^{-1}	5.114208×10^{-1}
160	0.527876260048	0.532846958416	0.528138528000	5.278763×10^{-1}	5.328470×10^{-1}
180	0.526626479114	0.534524507456	0.528138528000	5.266265×10^{-1}	5.345245×10^{-1}
199	0.517233880416	0.526050886543	0.521645022000	5.172339×10^{-1}	5.260509×10^{-1}

11. Conclusion

In this study, the dynamics of drinking behavior in a population were productively modeled and analyzed through a set of non linear mathematical equations using the Genocchi wavelet technique. Solid accuracy was demonstrated by the method and it is verified through theoretical analyses such as error bounds, convergence, existence, uniqueness, and boundedness of the solutions. A comparative assessment with the ABM technique is further extended to include the previous method that shows the efficiency of the Genocchi wavelet approach. Additionally, three-dimensional graphical representations were provided for varying fractional orders and including new visualizations covering different ranges of α. The 3D plot lies between the ranges $0 \leq \alpha \leq 1$, $1 \leq \alpha \leq 2$, $2 \leq \alpha \leq 3$, $3 \leq \alpha \leq 4$. The error analyses are also mentioned for each components with different values of α. In $M(t)$ and $R(t)$ when the order increase, the error is reducing. Overall, while both methods perform reasonably well the GW method demonstrates superior or equivalent accuracy across all three components. Superior accuracy is demonstrated by the proposed GW method, with consistently lower absolute error values obtained when compared to previously published methods and improved or comparable performance observed relative to the ABM scheme, thereby confirming its effectiveness and reliability. Also, the fractional-order model accurately captures the real data trend, with higher α values improving the approximation. The framework established in this study can be extended to analyze more complex models involving multi-dimensional and stochastic systems. Future research may focus on the application of the Genocchi wavelet method to other behavioral models or systems in epidemiology, economics, and ecology to evaluate its versatility and scalability.

Competing Interests
There is no conflict of interest.

Authors contribution statement
Jasinth Sylvia : Conceptualization, model design, empirical analysis, evaluation, software, interpretation. Surath Ghosh : Conceptualization, model design, empirical analysis, evaluation, validation, reviewed final draft.

Data availability and access
All data are available in the following link-
https://ourworldindata.org/alcohol-consumption.

Funding Declaration
There is no funding support.

References

[1] Waleed Mohamed Abd-Elhameed, Mohamed Salem Al-Harbi, Amr Kamel Amin, and Hany M. Ahmed. Spectral treatment of high-order Emden–Fowler equations based on modified Chebyshev polynomials. *Axioms*, 12(2):99, 2023.

[2] Khushbu Agrawal, Sunil Kumar, and Ali Akgül. An algorithm for numerical study of fractional atmospheric model using Bernoulli polynomials. *Journal of Applied Mathematics and Computing*, 70:3101–3134, 2024.

[3] Dan Aksim and Dmitry Pavlov. On the extension of Adams–Bashforth–Moulton methods for numerical integration of delay differential equations and application to the moon's orbit. *Mathematics in Computer Science*, 14:103–109, 2020.

[4] Zaileha Md Ali, Fatin Nadira Rusly, Nuramira Husna Abu Hassan, Nur Aziean Mohd Idris, Siti Rahimah Batcha, and Zubaidah Sadikin. SIR fractional order of simulated Covid-19 cases using Adams Bashforth-Moulton method. *Journal of Advanced Research in Applied Sciences and Engineering Technology*, 42(1):82–92, 2024.

[5] Badr Saad T Alkahtani, Khushbu Agrawal, Sunil Kumar, and Sara S Alzaid. Bernoulli polynomial based wavelets method for solving chaotic behaviour of financial model. *Results in Physics*, 53:107011, 2023.

[6] M Elarbi Benattia and K Belghaba. Numerical solution for solving fractional differential equations using shifted Chebyshev wavelet. *Gen. Lett. Math*, 3(2):101–110, 2017.

[7] Sanjay Bhatter, Amit Mathur, Devendra Kumar, and Jagdev Singh. A new analysis of fractional Drinfeld–Sokolov–Wilson model with exponential memory. *Physica A: Statistical Mechanics and its Applications*, 537:122578, 2020.

[8] Sung Kyu Choi, Bowon Kang, and Namjip Koo. Stability for Caputo fractional differential systems. In *Abstract and applied analysis*, volume 2014, page 631419. Wiley Online Library, 2014.

[9] Anupama Choudhary, Devendra Kumar, and Jagdev Singh. Numerical simulation of a fractional model of temperature distribution and heat flux in the semi infinite solid. *Alexandria Engineering Journal*, 55(1):87–91, 2016.

[10] Nuno Crokidakis and Lucas Sigaud. Modeling the evolution of drinking behavior: A statistical physics perspective. *Physica A: Statistical Mechanics and its Applications*, 570:125814, 2021.

[11] Cristopher Da Silva, Miriam Peces, Aldonza Jaques, Jose J Muñoz, Joan Dosta, and Sergi Astals. Fractional calculus as a generalized kinetic model for biochemical methane potential tests. *Bioresource Technology*, 396:130412, 2024.

[12] Kai Diethelm and Neville J Ford. Multi-order fractional differential equations and their numerical solution. *Applied Mathematics and Computation*, 154(3):621–640, 2004.

[13] Kai Diethelm, Neville J Ford, and Alan D Freed. Detailed error analysis for a fractional Adams method. *Numerical algorithms*, 36:31–52, 2004.

[14] A Karimi Dizicheh, S Salahshour, Ali Ahmadian, and Dumitru Baleanu. A novel algorithm based on the Legendre wavelets spectral technique for solving the Lane–Emden equations. *Applied Numerical Mathematics*, 153:443–456, 2020.

[15] Behzad Ghanbari and Devendra Kumar. Numerical solution of predator-prey model with Beddington-Deangelis functional response and fractional derivatives with Mittag-Leffler kernel. *Chaos: An Interdisciplinary Journal of Nonlinear Science*, 29(6), 2019.

[16] Surath Ghosh. Numerical study on fractional-order Lotka-Volterra model with spectral method and Adams–Bashforth–Moulton method. *International Journal of Applied and Computational Mathematics*, 8(5):233, 2022.

[17] Surath Ghosh. An analytical approach for the fractional-order Hepatitis B model using new operator. *International Journal of Biomathematics*, 17(01):2350008, 2024.

[18] Gokul Hariharan, K Kannan, and KR Sharma. Haar wavelet method for solving Fisher's equation. *Applied mathematics and computation*, 211(2):284–292, 2009.

[19] Md Monirul Islam, Zabir Al Nazi, ABM Aowlad Hossain, Md Masud Rana, et al. Data prediction in distributed sensor networks using Adam Bashforth Moulton method. *Journal of Sensor Technology*, 8(02):48, 2018.

[20] Toungainbo Cédric Kamdem, Kol Guy Richard, and Tibi Béda. Modeling the mechanical behavior of rock during plastic flow using fractional calculus theory. *Applied Mathematical Modelling*, 130:790–805, 2024.

[21] Hammad Khalil, Kamal Shah, and R Ali Khan. Approximate solution of boundary value problems using shifted Legendre polynomials. *Applied and Computational Mathematics*, 16(3):269–285, 2017.

[22] Adem Kilicman and Zeyad Abdel Aziz Al Zhour. Kronecker operational matrices for fractional calculus and some applications. *Applied mathematics and computation*, 187(1):250–265, 2007.

[23] Mustafa Kudu. A parameter uniform difference scheme for the parameterized singularly perturbed problem with integral boundary condition. *Advances in Difference Equations*, 2018:1–12, 2018.

[24] Sunil Kumar, Ranbir Kumar, MS Osman, and Bessem Samet. A wavelet based numerical scheme for fractional order SEIR epidemic of measles by using Genocchi polynomials. *Numerical methods for partial differential equations*, 37(2):1250–1268, 2021.

[25] Fei Li, Haci Mehmet Baskonus, S Kumbinarasaiah, G Manohara, Wei Gao, and Esin Ilhan. An efficient numerical scheme for biological models in the frame of Bernoulli wavelets. *Comput Model Eng Sci*, 137(3), 2023.

[26] Chandan Maji. Dynamical analysis of a fractional-order predator–prey model incorporating a constant prey refuge and nonlinear incident rate. *Modeling Earth Systems and Environment*, 8(1):47–57, 2022.

[27] Emine Misirli and Yusuf Gurefe. Multiplicative Adams Bashforth–Moulton methods. *Numerical Algorithms*, 57:425–439, 2011.

[28] Kolade M Owolabi. Modelling and simulation of a dynamical system with the Atangana-Baleanu fractional derivative. *The European Physical Journal Plus*, 133(1):15, 2018.

[29] Prabir Panja. Dynamics of a fractional order predator-prey model with intraguild predation. *International Journal of Modelling and Simulation*, 39(4):256–268, 2019.

[30] Jesus Peinado, J Ibáñez, Enrique Arias, and Vicente Hernández. Adams–Bashforth and Adams–Moulton methods for solving differential Riccati equations. *Computers & Mathematics with Applications*, 60(11):3032–3045, 2010.

[31] Bijil Prakash, Amit Setia, and Deepak Alapatt. Numerical solution of nonlinear fractional SEIR epidemic model by using Haar wavelets. *Journal of computational science*, 22:109–118, 2017.

[32] G Psihoyios and TE Simos. *Trigonometrically fitted Adams-Bashforth-Moulton methods for periodic initial value problems*. Elsevier, 2003.

[33] Parisa Rahimkhani and Yadollah Ordokhani. Performance of Genocchi wavelet neural networks and least squares support vector regression for solving different kinds of differential equations. *Computational and Applied Mathematics*, 42(2):71, 2023.

[34] Ana Caroline Raimundini Aranha, Rafael Oliveira Defendi, Maria Carolina Sérgi Gomes, Caroline Casagrande Sipoli, Danielli Andrea Nardino, Vitor Viganô Oliveira, Marcelo de Jesus Corte Rosalém, and Rúbia Michele Suzuki. Mathematical modeling of the drying and oil extraction processes of passion fruit seeds using fractional calculus. *Journal of Chemical Technology & Biotechnology*, 99(8):1800–1809, 2024.

[35] Joel A Rosenfeld and Warren E Dixon. Approximating the Caputo fractional derivative through the Mittag-Leffler reproducing kernel hilbert space and the kernelized Adams–Bashforth–Moulton method. *SIAM Journal on Numerical Analysis*, 55(3):1201–1217, 2017.

[36] Tasmia Roshan, Surath Ghosh, Ram P Chauhan, and Sunil Kumar. A robust study on fractional order HIV/AIDS model by using numerical methods. *Engineering Computations*, 40(7/8):1545–1569, 2023.

[37] Bhuvnesh Sharma, Sunil Kumar, Carlo Cattani, and Dumitru Baleanu. Nonlinear dynamics of Cattaneo–Christov heat flux model for third-grade power-law fluid. *Journal of Computational and Nonlinear Dynamics*, 15(1):011009, 2020.

[38] Ayesha Sohail, Khadija Maqbool, and Rahmat Ellahi. Stability analysis for fractional-order partial differential equations by means of space spectral time Adams-Bashforth Moulton method. *Numerical Methods for Partial Differential Equations*, 34(1):19–29, 2018.

[39] Pundikala Veeresha, Doddabhadrappla Gowda Prakasha, and Devendra Kumar. An efficient technique for nonlinear time-fractional Klein–Fock–Gordon equation. *Applied Mathematics and Computation*, 364:124637, 2020.

[40] Mingxu Yi, Jun Huang, and Jinxia Wei. Block pulse operational matrix method for solving fractional partial differential equation. *Applied Mathematics and Computation*, 221:121–131, 2013.

[41] Rahat Zarin, Hammad Khaliq, Amir Khan, Iftikhar Ahmed, and Usa Wannasingha Humphries. A numerical study based on Haar wavelet collocation methods of fractional-order antidotal computer virus model. *Symmetry*, 15(3):621, 2023.